A Reproducible Triple-Network Neurobiology of Depressive Rumination

Pisner, D.A.[1,2], Shumake, J.[1], Beevers, C.G.[1,2], Schnyer, D.M.[2]
[1] Institute for Mental Health Research (IMHR), 116 Inner Campus Dr. Austin, TX 78705
[2] Department of Psychology, University of Texas at Austin, 108 E Dean Keeton St, Austin, TX 78712

Corresponding Author Contact Information:
dpisner@utexas.edu; Phone: 703-200-8389, Mailing Address: 108 E Dean Keeton St, Austin, TX 78712
Short Title: Multimodal Discovery and Replication
Keywords: Multimodal; Microstructure; Resting-State; Triple-Network; Depressive Rumination; Reproducibility
Abstract word count: 222
Total word count: 9357
Figure count: 12
Table count: 2
Supplementary Material Count: 1 File

Abstract

Background: Depressive Rumination (DR), a cognitive style that involves a repetitive focus on one's distress, has been linked to alterations in functional brain networks including Default Mode, Salience, and Executive Control (DMN; SN; ECN). The underlying white-matter (WM) microstructure supporting these networks and their collective role in DR remains unknown, however.

Methods: Using diffusion MRI and resting-state BOLD fMRI, we explored multimodal relationships between DR severity, WM microstructural connectivity, and resting-state functional connectivity in depressed adults, and then replicated our results in a phenotypically-matched, independent sample.

Results: Across both samples ($N = 78$), DR severity was associated with: (a) global WM microstructure of the right temporal Superior Longitudinal Fasciculus (SLFT) along with distributed frontoparietal WM clusters of both primary and secondary-fiber types; (b) functional connectivity within and between the 'triple-network', consisting of three distinct subnetworks of DMN, SN, and ECN corresponding to self-reference, emotional salience, and attention engagement mechanisms of DR, respectively. In an unprecedented synthesis of these findings, we then discovered that the distributed WM disturbances in DR perpetuate the imbalance of functional segregation and integration of the triple-network in DR.

Conclusion: Ultimately, findings converged across four separate methodologies and only those effects which were sufficiently powered fully-replicated across samples. Taken together, our results serve to unify and extend existing work by providing reproducible support for a microstructural-functional 'triple-network' neurobiology of trait rumination in depression.

Cognitive models of depression posit that negatively biased self-referential processing plays a critical role in maintaining the disorder[1]. Depressive Rumination (DR) is the perseverative form of this cognitive bias, which involves a repetitive focus on "one's depressive symptoms and on the implications of those symptoms"[2]. DR has been shown to significantly contribute to depressive symptom severity[2], duration[3], and relapse likelihood[4] across multiple forms of depression. Despite its central role in depression maintenance, there are few effective treatments for DR[5,6]. By delineating reproducible neurobiological models of DR, researchers might better understand underlying vulnerabilities, identify more precise treatment targets, and develop more effective neurocognitive interventions for depression[7,8].

A Triple-Network Model of Depressive Rumination

At the core of DR is *self-referential processing*[9], which is inwardly directed attention focused on the self. This mechanism is associated with functional activation of modular cortical areas, such as the Precuneus[10] along with the anterior and posterior cingulate cortices (ACC; PCC)[11]; each of these areas has been associated with self-focused cognitive processes that include thought-suppression, mentalization, and prospection[12–15]. Although few studies have explored grey matter structural biomarkers of self-reference, reduced cortical volume of the Precuneus is known to be associated with autobiographical memory disturbances[16,17] and poor metacognition[18,19].

Since self-referential processing is believed to predominantly operate in a task-negative brain state[20], studies that employ resting-state functional MRI (rsfMRI) are believed to offer deeper insights into the neurobiology of self-reference[9,21]. Indeed, rsfMRI has enabled researchers to more broadly attribute self-referential processes to the Default-Mode Network (DMN), whose functional connectivity may reflect mind-wandering[20,22] and for which the Precuneus is a core hub[23]. Precise features that differentiate "healthy" mind-wandering from maladaptive ruminative patterns are difficult to distinguish, however, perhaps due to the inherent subjectivity of inner mentation along with fundamental limitations of the resting-state modality in general[24]. Nevertheless, increased DMN activity during internally-focused attention is generally believed to amplify self-referential processing and thereby increase the demand on cognitive resources[25,26]. In particular, recent studies have shown that greater DR severity is associated with lower functional connectivity within a parietal sub-system of the DMN, the Precuneal DMN (pDMN), which is both vulnerable to malfunctioning under conditions of cognitive resource depletion[27], and specifically responsible for regulating the episodic memory retrieval that supports inner mentation[20].

Emotional salience, a second proposed mechanism of DR, may be necessary for assigning a negative bias to self-referential processing. A wealth of literature has shown that emotional salience is associated with both the function and structure of the ACC, Insula, and Amygdala, and can extend to other regions as well[28,29]. Greater sustained activation within the Amygdala has been observed, for example, in response to negative-valence words following non-emotional words in depressed individuals[30]. Whereas the amygdala may act as a source of emotional signaling[31], the ACC assigns salience to emotional signals in the service of goal attainment[32]; in the context of DR, for instance, such goals might include relief from depressive symptoms. Research into the precise role of the ACC in DR have been mixed, however[9,12,33]. On the one hand, such discrepancies may reflect the variety of motivational states that are engaged during different task paradigms[34], but they might also allude to its dense interconnectivity with other cortical areas[32] or the multiple specialized functions among sub-regions of the ACC itself[35]. Thus, emotional salience in DR may be more precisely understood within a functional connectivity perspective of the Salience Network (SN)[36].

In fact, a recent study on depressed teenagers found a critical role for the SN in the maintenance of negative cognitive bias and self-criticism in DR[57]. One reason for this finding may be that aberrant functional connectivity of the SN during self-referential processing results in misappropriated "tagging" of self-relevant thoughts with a negative bias[9], perhaps through dysregulated reward circuitry[38]. Along these lines, a recent task-based fMRI study showed that depressed ruminators tend to more actively recruit SN nodes simultaneously during reward anticipation. Hence, emotional salience in the context of DR might also or alternatively be construed as a hypervigilance to self-relevant cues[39].

A third proposed mechanism of DR is impaired *attentional engagement*, which may instantiate repeated failures to disengage from negatively-salient self-referential processing while also preventing attentional shifts toward neutral or positive thoughts[40]. In depressed individuals, this impaired disengagement[40–42] is believed to amplify and sustain the negative bias of self-referential processing by spurring a vicious cycle of self-criticism that drains the cognitive resources needed to counteract the increase[37]. Thus, the mechanism of impaired disengagement may lend explanation to the perseverative nature of DR, which distinguishes it from more adaptive, reflective forms of rumination[4,43]. Broadly construed, impaired disengagement in DR likely implicates the aberrant structural and functional properties of cognitive control modules, such as the dorsolateral and inferior prefrontal cortices[12,44,45], whose activation patterns are largely titrated by the ACC[32]. Accordingly, the functional connectivity perspective delineates a frontal Executive Control Network

(fECN), which encompasses each of these cortical areas and may help to better conceptualize the broader role of impaired disengagement in DR.

Perhaps in light of the three proposed mechanisms of DR, the three corresponding resting-state networks (RSNs) previously discussed have become ubiquitous in the study of DR's functional neurobiology—the DMN, SN, and ECN[36,37]. Nevertheless, the three proposed mechanisms of DR are often discussed as competing, rather than complementary, theories of its etiology[6]. Accordingly, the three corresponding RSN's have been studied largely in isolation – i.e. with respect to their *within-network* functional connectivity patterns[9,36] – in the context of DR research[9].

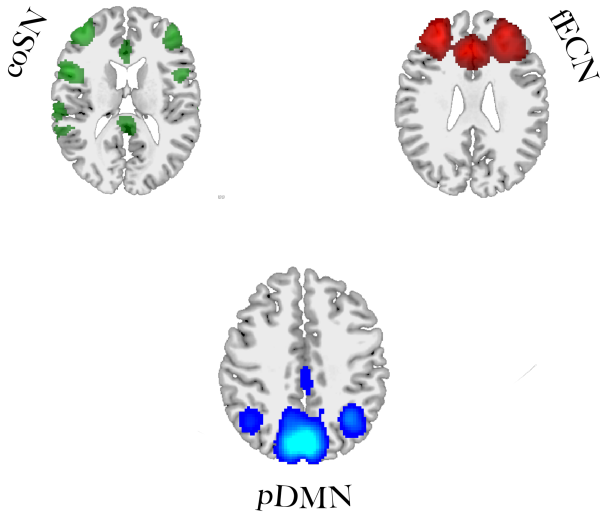

Figure 1: Three resting-state networks (RSNs) are discussed independently in prior studies on DR: the Cingulo-Opercular Salience Network (SN) shown in green, the frontal Executive Control Network (ECN) shown in red, and the Precuneal Default Mode Network (pDMN) shown in blue. These three networks are also described collectively as belonging to the frontoparietal triple network, and their functional properties coincidentally correspond to the three proposed mechanisms of DR, which include self-referential processing, emotional salience, and cognitive control, respectively.

Despite their diverse specialized intrinsic functions, however, mounting research has shown that the DMN, SN, and ECN largely interact with one another[46]. Hence, additional insights might be gleaned by studying these particular RSN's as a mesoscale system of networks – the "triple network" – as some have already proposed more broadly in the study of depression[46–49] (*See* **Figure 1**). In fact, only one study to date has explored *between-network* functional connectivity patterns in DR[50]. Specifically, Hamilton et al. (2011) used state-change analysis of rsfMRI to show that higher DR severity is associated with greater DMN dominance over the ECN, with a variable role for the SN across differing levels of depression severity[50]. That study did not include structural brain measures, however, which are still needed to explain DR's persistence as a stable trait[54]; likewise, due to its limited sample size (N=34), the generalizability of its findings are unclear.

Microstructural and Functional Connectivity Models of Depressive Rumination

Studies have shown that inter-individual differences in DR severity likely indicate the existence of structural brain correlates of DR[9,12,44,53]. Given that the perseveration implicated in DR

is a relatively stable trait[54], it would therefore also seem to implicate a complex structural basis in white matter (WM) microstructure, and not just modular grey matter cortices[44]. It follows that the structural analogue to functional connectivity is microstructural connectivity[55], which is based on anisotropic properties of WM in the brain. In fact, BOLD signal clustering of resting-state WM has been shown to generate patterns resembling white-matter tracts[56]. WM pathways can be studied using methods like diffusion tensor MRI (dMRI), which provides an *in vivo* method for measuring global and local Fractional Anisotropy (FA) that likely approximate microstructural connectivity[57]. Although recent studies beyond DR literature have shown that WM microstructural connectivity of frontoparietal tracts, such as the Cingulum (CCG) and the Uncinate Fasciculus (UF), may support the DMN[58] and ECN[59], respectively, only one study to date has explicitly investigated the WM basis for DR[58]. That study used Tract-Based Spatial Statistics (TBSS) to show that FA of the Superior Longitudinal Fasciculus (SLF) and neighboring motor fibers was negatively associated with DR.[53] Due to the small sample size of that study (n = 16), however, it may also not be possible to generalize its results to other depressed populations[58].

A Systems-Level Understanding of Depressive Rumination

Overall, DR's neurobiology is likely characterized by a variety of neural biomarkers that operate across multiple levels of neural complexity, encompass both structural and functional dimensions, and correspond to at least the three proposed cognitive mechanisms of DR. Although studies on modular biomarkers have identified a core set of nodes relevant to each of these mechanisms, the modular perspective cannot account for dynamic interactions among those nodes[62]. To capture more precise brain-cognition relationships relevant to DR, connectivity biomarkers identified across both functional[36,63] and structural[53] modalities[64,65] may be maximally informative. Likewise, neuroscientific appeals made to either structural or functional connectivity biomarkers of DR, considered in isolation, could reduce the precision of our etiological understanding[66]. Hence, multimodal studies of microstructural and functional connectivity, considered in tandem, might help to clarify any systems-level[67] mechanisms responsible for maintaining DR as a stable trait[68–70].

In the present study, we propose two hypotheses: 1) a microstructural-functional neurobiology of trait DR exists and implicates both frontoparietal microstructural connectivity and triple-network functional connectivity, corresponding to each of the three proposed cognitive mechanisms of DR—aberrant self-referential processing, negatively-biased salience processing, and impaired disengagement of attention; 2) individual differences in trait DR can be explained

127 multimodally—that is, through joint appeal to triple-network functional connectivity with respect to
128 underlying microstructural connectivity constraints.
129 To test and explore these hypotheses, we utilize data from two neuroimaging modalities,
130 dMRI and rsfMRI. Given the absolute importance of replication in cognitive neuroscience[71] and the
131 growing need for more credible and reproducible neurobiological models of disordered cognition[72],
132 we additionally perform our analyses across two separate datasets, acquired independently and at
133 different locations. This approach, which is rarely used in social or biological sciences[71], enabled us
134 to employ hypothesis testing to determine whether initial discovery findings could be directly
135 replicated in a second independent sample. The findings that did replicate would, in turn, afford a
136 higher degree of confidence in support of our conclusions, and perhaps provide an auxiliary means
137 of inferring generalizability beyond statistical power alone[73].
138 We test our first hypothesis by applying multiple linear regression analyses to dMRI and
139 rsfMRI data independently, to identify any microstructural and functional connectivity biomarkers
140 of DR, respectively. The dMRI analyses include both TBSS and global probabilistic tractography
141 methods[57], whereas the rsfMRI analyses encompass both within-network and between-network[74]
142 resting-state functional connectivity based on Independent Components Analysis (ICA)[36]. We then
143 test the second hypothesis by jointly examining microstructural-functional connectivity
144 relationships associated with DR. Lastly, we test both of our hypotheses by applying a similar
145 analytic pipeline developed for the discovery sample to an independent sample obtained from NKI
146 Rockland[73,75].

147 **METHODS**

148 ***Participants – Discovery sample***

149 Thirty-nine treatment-seeking participants with DSM-IV Major Depressive Disorder (MDD)
150 were recruited for this study from advertisements placed online, in newspapers, and on late night
151 TV. Participants were screened for medical or physical conditions that would preclude participation
152 in an MRI study. They also completed an abbreviated Mini International Neuropsychiatric
153 Interview (MINI)[76] to determine provisional MDD diagnosis, which were then confirmed using in-
154 person Structured Clinical Interviews for the DSM-IV Disorders (SCID)[77] administered by a trained
155 research assistant. Participants were excluded if they met criteria for past year substance abuse or
156 dependence, current or past psychotic disorder, bipolar disorder, and schizophrenia. Participants
157 receiving pharmacological treatment were allowed into the study if there has been no medication

change in the 12 weeks prior to study entry. To minimize brain changes associated with aging, individuals were between the age of 18 and 55[78].

Ethics Statement

The Institutional Review Board at the University of Texas at Austin approved all study procedures and materials and all participants provided signed informed consent.

Depressive Rumination Measurement

The RSQ (Response Styles Questionnaire)[79] is a 10-item self-report measure of the tendency to ruminate. It consists of a total score and two sub-scales: reflection and brooding. The reflection subscale measures an individual's tendency to turn inward to engage in problem-solving and thereby alleviate negative or depressed mood[4], whereas brooding measures the maladaptive form of rumination believed to be a proxy for DR[4,50]. Brooding specifically reflects the intensity of ruminative responses to expressions of negative emotion[2]. For each item, subjects indicate the frequency of each event on a scale ranging from 0 ("almost never") to 3 ("almost always"), yielding a range of possible scores from 0-30. The brooding subscale has high reliability (α=0.77-0.92)[79], is well-validated within depressed populations[80], decontaminated of any explicitly depressive content[80], and the sub-scale of choice for most neurobiological studies of DR[9,20,36,40,50]. For these reasons, we used the brooding subscale exclusively to measure DR.

Depression Severity Measurement

The Beck Depression Inventory (BDI)[81] is a 21-item self-reporting questionnaire for evaluating the severity of depression in normal and psychiatric populations. It contains 21 items on a 4-point scale from 0 (symptom absent) to 3 (severe symptoms), and instructs the participant to recall depression symptoms occurring over the previous two weeks.

Imaging Acquisition

MRI scans were acquired on a whole body 3T GE MRI with an 8-channel phase array head coil. The scanning protocol involved collection of a localizer followed by a high-resolution T1 structural scan, two resting state scans of 6 minutes each, a second high-resolution structural scan, and finally a 55-direction diffusion tensor (dMRI) scan. For the resting-state scan, instructions were presented utilizing a back-projection screen located in the MR bore and viewed through a mirror mounted on the top of the head coil. Participants were instructed to remain awake and alert and keep their gaze on a fixation cross (+) presented approximately at the center of their field of view for the 6-minute duration of the scan. (*See* **Appendix, Methods: Section A***)*.

dMRI Preprocessing

Preprocessing of Diffusion Magnetic Resonance Imaging (dMRI) data was carried out using a custom preprocessing workflow that included eddy correction, brain extraction, denoising, and tensor/ball-and-stick model fitting tools adapted from the FMRIB Diffusion Toolbox[82]. To achieve maximal sensitivity and specificity from the dMRI data, preprocessing included rigorous automated and manual quality control steps (*see* **Appendix, Methods: B**).

dMRI: Tract-Based Spatial Statistics (TBSS) / Tractography and DR

A number of approaches to dMRI analysis were implemented. To begin, the whole-brain data was interrogated using Tract-Based Spatial Statistics (TBSS)[83] to identify microstructural characteristics that were associated with brooding severity (*see* **Appendix, Methods: Section C**). We additionally employed the 'crossing-fibers' extension of TBSS[84], which is less often used due to its computational expense, but can uniquely capture group differences in crossing fibers (i.e. "secondary" fibers), unlike TBSS based on the tensor model alone.

For statistical testing, a permutation approach was employed using FSL's "randomise" function with the TFCE Threshold-Free Cluster Enhancement option, generating 10,000 permutations and applying family-wise error (FWE)-correction to obtain cluster inferences. A two-tailed regression model was next generated using FSL's GLM function, whereby RSQ brooding scores were used as the criterion variable with age and gender as nuisance covariates. Age was included due to a well-known confounding influence of age on WM microstructure[85], and gender was included due to some evidence of gender differences in rumination—namely, that females tend to exhibit greater rumination severity than males[86]. The resulting negative contrast mask (i.e. representing those voxels negatively associated with greater DR severity) was thresholded twice—first at p=0.05 and again at p=0.01. The use of two thresholds allowed us to determine those voxels which were most strongly associated with DR (p=0.01), while also yielding a more liberal cluster of voxels (p=0.05) that could be reliably used as a Region-of-Interest (ROI) for multimodal analysis.

Following TBSS, we sought to corroborate our initial group level, voxel-wise dMRI findings using individual-level tractography, which is an alternative dMRI methodology that attempts to reconstruct known WM pathways while retaining each subject's image in native space orientation. Since spatial information is not manipulated in tractography as it is with TBSS[87], tractography could confirm any TBSS findings in native space, while also disconfirm false-positives due to non-physiological factors such as image misalignment, movement, and other factors resulting from the methodological limitations of TBSS[88].

For tractography, we chose to analyze average FA measures from the entire pathways of tracts of interest whose labels included significant voxels from the earlier TBSS stage. These measures were then further analyzed across hemispheres to establish any significant laterality effects[89]. To perform tractography, we specifically used the TRActs Constrained by UnderLying Anatomy (TRACULA) tool in FreeSurfer (version 5.3.0)[57], which delineates 18 known WM bundles using each participant's joint dMRI and T1-weighted MRI data (*See* **Appendix, Methods: Section D**).

rsfMRI Preprocessing

Preprocessing of baseline rsfMRI data was carried out using a custom workflow based on FSL's FEAT[82], combined with AFNI and FREESURFER tools. Additional denoising steps were taken by controlling for WM and ventricular CSF confounds, and by using FSL's ICA-based Xnoisifier artifact removal tool (FIX) to control for motion and physiological artifact (*See* Appendix, Methods: **Section E**).

rsfMRI: Group Independent-Components Analysis (ICA) / Dual-regression and DR

Group-level Independent Components Analysis (ICA) was performed by employing "temporal concatenation" of the complete, preprocessed rsfMRI time-series from all of the participants and restricted to twenty-five independent component (IC) outputs[90]. Four IC's were manually identified as noise and removed from further examination. Of the remaining twenty-one networks, all were identified using visual inspection by way of reference to the 17 RSN's delineated by the Yeo et al. 2011 atlas[91], thus allowing for identification of the three IC's of the triple-network that were introduced above - the pDMN[20,50], the coSN[47], and the fECN[37,92,93].

A dual-regression approach[94] was next performed on the triple-network RSN's, which were used as regressors for each individual subject's 4D set of fMRI volumes in order to extract time-series that were both specific to each subject and to each of the three IC's[64]. Design matrices and contrasts were then created to test for correlations between brooding severity and total average intrinsic connectivity within each of these RSN's, controlling for age and gender. These regression models were tested separately for each RSN, using two-tailed contrasts in an identical manner to that used in TBSS, with FSL's randomise (10,000 permutations) and TFCE cluster-thresholding with whole-brain FWE-correction[95]. To further correct for analysis-level multiple comparisons among the three triple-network RSN's, we also Bonferroni-corrected our alpha significance level for these models to 0.05/3 or p=0.0167.

254 ***Between-Network Functional Connectivity and DR***

255 To investigate interactions between the triple-network RSN's, we utilized FSLNets[96], a
256 MATLAB-based tool that interfaces with FSL. FSLNets utilizes the individual resting-state network
257 IC's generated from the earlier dual-regression stage to perform hierarchical clustering across
258 RSN's and estimate a partial-correlation (Spearman's ρ) matrix for each RSN for each participant.
259 To perform between-RSN general linear modeling, randomise was again employed with FWE-
260 correction, but this time using the nets_glm function at 10,000 permutations. The design matrices
261 and contrasts used in the earlier FSL GLM analyses, were used in this analysis as well. In summary,
262 whereas the dual-regression approach identified DR-associated clusters (both *belonging to* and
263 *external to* the RSN's) that are more strongly connected to each of the triple-network RSN's
264 considered separately, the FSLnets approach identified DR-associated patterns of between-network
265 correlation among the triple-network RSN's considered collectively.

266 ***Replication and Statistical Power***

267 To formally test whether the findings would generalize beyond the discovery sample[73], we
268 directly replicated all stages of analysis using a phenotypically similar, independent sample
269 obtained from the publicly-available, multi-site NKI Rockland dataset[75]. By chance, that dataset
270 contained a sub-sample of participants with equivalent demographics to those participants from our
271 original sample; this included (*N*=39) participants who were between the ages of 18-55, had no
272 history of drug abuse or severe comorbid psychopathology, had both useable dMRI data and rsfMRI
273 data, and reported at least some depressive symptomatology. The participants had also been
274 administered the 21-item Beck Depression Inventory (BDI-II) and the 22-item Rumination
275 Response Scale (RRS)(*See* **METHODS: Depressive Rumination Measurement**), which
276 contained identical brooding sub-scale items to those administered in the 10-item RSQ scale[80]. As
277 part of a larger battery of measures, many but not all participants also completed the Structured
278 Clinical Interview for DSM-IV-TR Axis I Disorders (SCID)[97]. Specifically, 33% of the n=39
279 participants met full criteria for MDD (18% current/recurrent and 15% in remission), requiring that
280 the remaining participants be included on the basis of broader depressive symptomology. This
281 included 66% with dysphoria as determined by elevated BDI-II scores (≥4)—a cutoff used in prior
282 studies[98,99]. One advantage to including dysphoric participants was that it could possibly allow us to
283 infer whether any replicated biomarkers of DR are specific to DR and not merely conflated with the
284 depressive symptoms specific to an MDD diagnosis.

Furthermore, to minimize the possibility of sample-variant effects due to incongruence of neuroimaging acquisition parameters across samples[100], we spatially and temporally resampled the rsfMRI and dMRI data in the replication sample to match the voxel resolution of the rsfMRI and dMRI data and the sampling frequency (i.e. TR) of the rsfMRI data in the discovery sample (*See* **Appendix, Methods: Sections F & G**). To ensure direct equivalence of neuroimaging data preprocessing in the replication[101], we also applied a nearly equivalent analytic pipeline to that applied to the discovery sample, but using the pDMN, fECN, and coSN group-ICA RSN definitions from the discovery dataset. Lastly, given the multiple scanner sites used to collect the neuroimaging data in the Rockland sample, we employed mixed-effects regression models (both with FSL's GLM and in R), whereby scanner site was additionally modeled as a random effect.

Since generalizability was a core aim of our study, power analyses were also conducted for detecting a large effect size when using multiple regression with two covariates (age and gender) and a significance level of $\alpha<0.05$ (*See* **Appendix: Methods, Section H**). Given our sub-optimal sample-sizes, we also opted to filter significant findings by a large effect size cutoff of $R^2=0.25$ for non-voxel-wise tests (i.e. tractography, multimodal analysis of beta-coefficients) and $p<0.01$ FWE-corrected threshold for voxel-wise tests (TBSS, Dual-Regression, FSLnets). This step would serve to more stringently identify those findings with the highest putative generalizability as well as those at risk of replication failure. Further, we classified a finding as being a 'full replication' if it replicated with respect to both equivalence in directionality of the effect and the RSN's or anatomical location(s) implicated. Likewise, the fully-replicated findings needed to meet our effect-size cutoff in at least one of the two samples, as well as an FWE-corrected $\alpha<0.05$ level of significance or uncorrected $\alpha<0.001$ level of significance for ROI analyses. Finally, to evaluate analysis-level false-discovery across multimodal replications, we further generated a null-distribution for post-hoc meta-analysis based on replication counts (*See* **Appendix: Methods, Section I**).

316 **RESULTS: INITIAL SAMPLE**

317 **Descriptive Statistics and Behavioral Findings**

318 Depressive rumination severity (DR) as measured using the RSQ was normally distributed
319 (*M*= 9.08, *SD*= 3.01, range: 17-48, IQR=5; Shapiro-Wilk = 0.976, p = 0.53). Depression severity
320 was also normally distributed (*M*= 31.94, *SD*= 8.16, range: 1-15, IQR=10, Shapiro-Wilk = 0.976, p
321 = 0.35) and was modestly associated with DR severity (R^2 = 0.13, $F(1, 37)$ = 5.61, p=0.02). Age
322 was positively skewed (*M*=27.51, *SD* = 8.80, range: 18-52) due to an overrepresentation of young
323 adults in our discovery sample. Although age was weakly correlated with RSQ brooding scores (R^2
324 = 0.09, $F(1, 37)$ = 3.84, p<0.06) and interacted with several neuroimaging measures throughout our
325 analyses, no significant interactions with gender were observed in either discovery or replication
326 samples. Nevertheless, we retained both age and gender as nuisance covariates for each regression
327 model to ensure maximal generalizability of our findings and consistency in our analyses.
328

329 **White Matter (WM) Microstructure and Depressive Rumination**

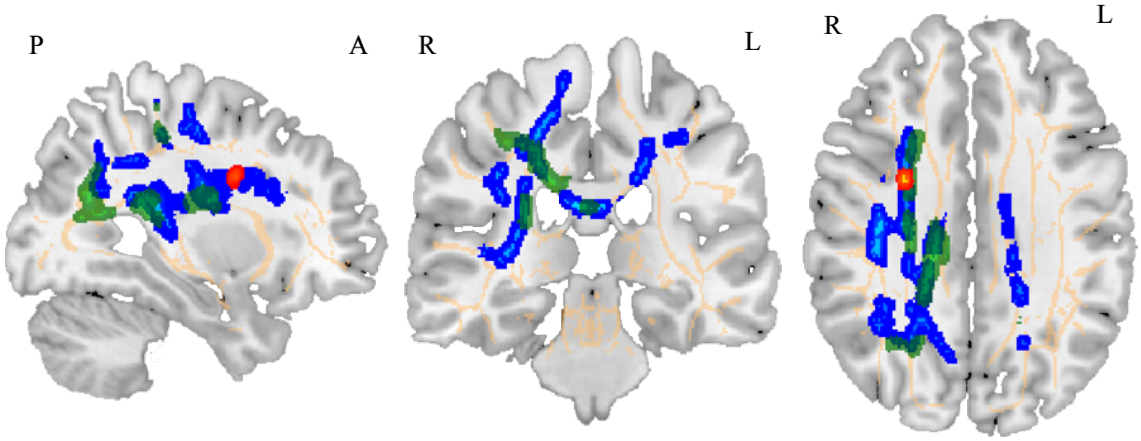

Figure 2: Depressive rumination was associated WM integrity primarily within the temporal and parietal parts of the right SLF including the anterior and posterior Corona Radiata, as well as the right posterior and anterior Cingulum along with the bilateral CST, particularly near its intersection with the posterior Corona Radiata. Here, significant associations with FA (p<0.01) are depicted in blue, significant associations with the F1 partial volume (p<0.01) are depicted in green, and significant associations with the F2 "crossing-fibers" volume in the superior at the Corona Radiata (p<0.01) are depicted in red-yellow. Note too that the FA and F1 clusters are, for the most part, overlapping; this indicates convergence across deterministic and probabilistic diffusion models. Since these measures capture fractional anisotropy of dominant diffusion direction(s) at each voxel, we should also expect them to track each other closely as a confirmation that any detected effects are not the result of corrupted model estimation, or other methodological errors.

330 ***TBSS: Localized White-Matter Biomarkers of DR***

331 Our first set of analyses employed tensor and crossing-fiber variations of TBSS to test for
332 WM microstructural connectivity biomarkers of DR (*see* **METHODS: TBSS; Appendix,**

Methods: Section C). Results first revealed significantly lower FA in association with higher brooding scores within the right Superior Longitudinal Fasciculus (SLF, both parietal and particularly temporal parts), the Cingulum, and the Corticospinal Tract (CST) (p<0.01 FWE; p<0.05 FWE; *see blue FA and green F1 clusters in* **Figure 2**). Some of these voxels also extended into the Anterior Thalamic Radiation (ATR), Uncinate Fasciculus (UF), and Splenium (p<0.05 FWE; p<0.05 FWE; p<0.05 FWE). A subsequent 'crossing-fibers' TBSS analysis closely tracked these findings, but further revealed significant relationships between DR and the microstructure of secondary-fibers (captured by the F2 partial volume) in a small cluster of the right superior Corona Radiata where the SLFT intersects with the Corpus Callosum at the Centrum Semiovale (p<0.01 FWE; *see red cluster in* **Figure 2***)*.

Tractography: Globalized White-Matter Biomarkers of DR

Using global probabilistic tractography, we next sought to both methodologically triangulate our TBSS findings and clarify the "mereology" of DR-associated WM pathways (i.e. their globality vs. locality). Given that TBSS analysis is performed on images where the WM tracks are aligned with an MNI standard, we performed probabilistic tractography on an individual subject basis to provide converging evidence that our findings are not driven by spatial normalization[57]. Using six pathways of interest from the outputs of TRACULA, including the right SLFT (Temporal part), right SLFP (Parietal part), CCG, CST, ATR, and Splenium, and Bonferroni Correction for the six tracts tested ($p_{corrected}$=0.05/6 = 0.0083), we found a robust negative association between weighted average FA of the right SLFT and DR severity (adj. R^2 = 0.18, $F(3, 36) = 3.85$, p<0.005). This clarified the findings conducted on a voxel-wise (i.e. on spatially normalized) basis with TBSS, by suggesting that the right SLFT may be both globally and locally associated with DR severity, whereas the other DR-associated pathways may be better construed as localized WM clusters.

Tract Hemisphericity

The aforementioned TBSS and tractography analyses indicated that the SLFT WM finding was distinctly right-lateralized. To test this formally, we treated hemisphere as a within-subjects measure and used Analysis of Variance (ANOVA) to compare two GLM's predicting DR for each tractography measure of global average FA. Specifically, the first GLM used left hemisphere as the predictor, whereas the second GLM used right hemisphere as the predictor, controlling for left hemisphere. From this analysis, we found supportive evidence for right lateralization of the SLFT ($F(36,1)=8.71$, p=0.005).

‘Within-Network’ Functional Connectivity and Depressive Rumination

Dual-Regression Findings

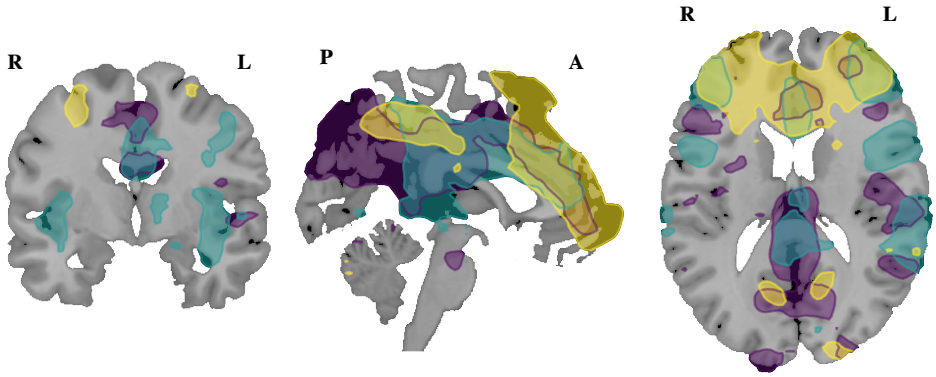

Figure 3: The above slices depict the three triple-network RSN’s resulting from group Independent Component Analysis (ICA) in the discovery sample. The fECN is shown in yellow, pDMN in purple, and coSN in turquoise. These same RSN definitions were used across both discovery and replication samples.

We next tested whether DR was associated with resting-state functional connectivity of the three triple-network RSN's as identified from the outputs of group-ICA followed by dual-regression (*see* **Figure 3** & **METHODS: rsfMRI Group-ICA** & **Dual-regression**). Results revealed that DR was highly correlated with functional connectivity in multiple clusters, some of which belonged to each respective triple-network RSN (i.e. ‘intrinsic’ connectivity), but also others that were outside of the respective RSN’s (i.e. ‘extrinsic’ connectivity) (*see* **Figure 4**). With respect to the latter, we found that DR was positively associated with extrinsic connectivity between the frontal Executive Control Network (fECN) and a small cluster (voxels=15) located at a juncture between the left

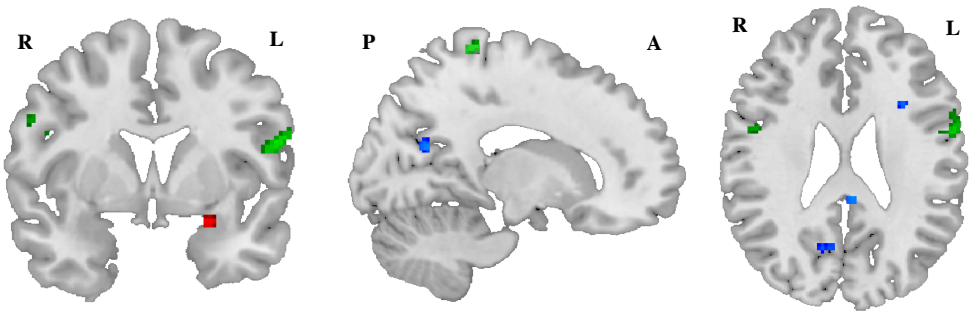

Figure 4: Significant clusters that exhibited lower functional connectivity within the pDMN associated with DR are depicted in blue, and include the PCC, Precuneus, left Precentral Gyrus, left Somatosensory Cortex, and the left inferior Frontal Gyrus. Significant clusters exhibiting lower functional connectivity within the coSN are depicted in green and include the dorsal left Precentral Gyrus, right superior Postcentral gyrus, left inferior Frontal Gyrus, and Broca’s area bilaterally. Finally, significant clusters exhibiting greater functional connectivity within the fECN are depicted in red and include the left Amygdala and left Parahippocampal Gyrus.

375 Amygdala and Parahippocampal Gyrus (p<0.05 FWE**;** *see red clusters in* **Figure 4**). Additionally,
376 the Precuneal Default Mode Network (pDMN) exhibited lower extrinsic connectivity with the left
377 somatosensory areas, left Precentral Gyrus and left inferior Frontal Gyrus (p<0.01 FWE; *see blue*
378 *clusters in* **Figure 3**), but also lower intrinsic functional connectivity between the Precuneus and
379 PCC. Lastly, the Cingulo-Opercular Salience Network (coSN) exhibited lower intrinsic functional
380 connectivity among the dorsal left Precentral Gyrus, left inferior Frontal Gyrus, right superior
381 Postcentral Gyrus, and most prominently in Broca's area bilaterally (p<0.01 FWE ; *see green*
382 *clusters in* **Figure 4**).

383 ***WM Microstructural and 'Within-Network' Functional Connectivity***

384 We next extracted the beta coefficients
385 representing average total connectivity
386 (intrinsic and extrinsic) for each of the DR-
387 associated triple-network clusters discovered
388 through dual-regression. This step would in
389 turn allow us to test for any multimodal
390 relationships between the within-network
391 functional connectivity findings and the
392 microstructural connectivity findings (i.e.
393 informed by tractography and TBSS). To
394 accomplish this, we first created a matched
395 subsample of n=32 subjects, since seven
396 subjects did not have both useable rsfMRI and
397 TRACULA data. As an initial step, we tested
398 for any associations between the dual-
399 regression clusters and average FA extracted
400 from the thresholded (p=0.05) negative
401 contrast mask from TBSS. That analysis
402 revealed that average FA negatively predicted
403 within-network functional connectivity of the pDMN and coSN (adj. R^2 = 0.14, $F(3, 29)$ = 2.75,
404 p<0.05; adj. R^2 = 0.03, $F(3, 29)$ = 1.33, p=0.06), but not the fECN.

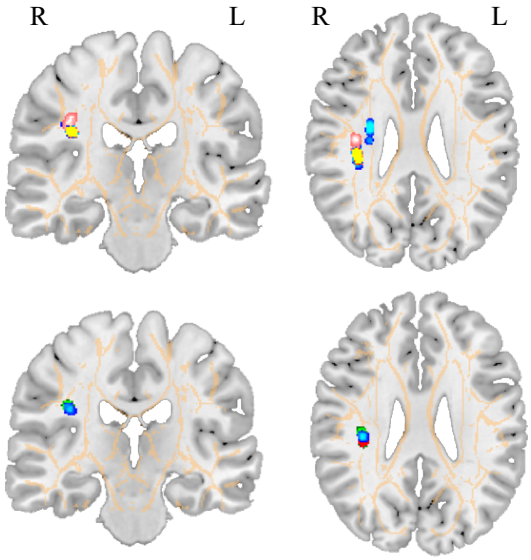

Figure 5: The above images depict correlations between RSN intrinsic/extrinsic functional connectivity and FA of the DR-associated right SLF fibers. The top row of images depicts a negative correlation between right medial SLFT FA and intrinsic connectivity of the coSN (pink) and pDMN (blue), as well as a positive correlation between FA and extrinsic connectivity of the right fECN (yellow) with the left Amygdala. The bottom row of images depicts the positive correlation between FA of secondary-fibers and these same intrinsic/extrinsic functional connectivity relationships.

Next, we tested an additional voxel-wise TBSS analysis with average total connectivity beta coefficients as regressors. From that analysis, we found that FA within a small cluster in the medial SLFP was also found to significantly predict total average connectivity of each of the triple-network RSN's (p<0.05, FWE)(*See light blue cluster* **Figure 5**). We also found that FA of a posterior cluster of the right SLFP was positively associated with functional connectivity of the fECN, whereas the medial cluster of the right SLFP was negatively associated with functional connectivity of both the pDMN and coSN (*see* **Figure 5**). We also found that secondary fiber FA in that same right medial SLFT region (i.e. posterior to the DR-associated secondary-fiber cluster described earlier) was positively associated with each of the triple-network RSN's ($R^2 = 0.35$, $F(3, 32) = 6.65$, $p<0.001$**;** adj. $R^2 = 0.24$, $F(3, 32) = 4.28$, $p=0.001$**;** adj. $R^2 = 0.20$, $F(3, 32) = 3.68$, $p<0.01$). That is, localized right SLFP primary and secondary fibers predicted the DR-associated within-network functional connectivity clusters of the triple-network. Since the TRACULA results only provided global measures of FA, averaged across the entire pathway and hence not sensitive to localized clusters, we additionally used the JHU White-Matter atlas to create atlas-labeled ROI's from the significant TBSS clusters (p=0.05 FWE). We could then use these ROI's to perform a supportive analysis on a

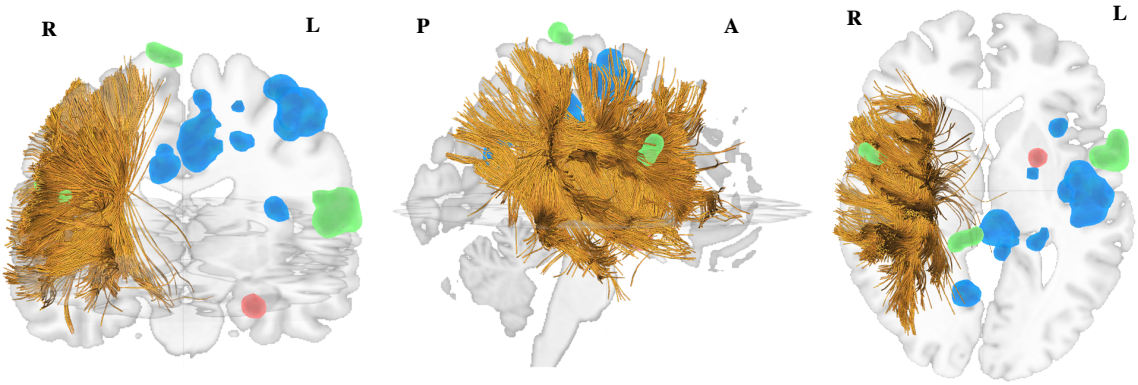

Figure 6: For multimodal visualization, right SLFT fibers are depicted above with orange streamlines alongside the significant dual-regression clusters (p<0.05 FWE) of the triple network, which are shown in blue, green, and red. The anterior left amygdala, whose positive extrinsic connectivity with the fECN was positively associated with DR, is displayed in red. The right Precuneus, PCC, inferior Frontal Gyrus, and left somatosensory areas, whose negative intrinsic/extrinsic connectivity patterns were positively associated with DR, is displayed in blue. Lastly, the left Precentral Gyrus, left inferior Frontal Gyrus, and Broca's area, whose negative intrinsic connectivity was positively associated with DR, are displayed in green.

non-voxelwise basis. Specifically, this approach would also allow us to explore whether applying atlas definitions to our original TBSS analysis with DR might afford greater specificity into multimodal structural-functional links (*See* **METHODS: TBSS**). That analysis further revealed that the DR-associated WM clusters of the CCG, ATR, UF, and Splenium each predicted functional connectivity of the DR-associated triple-network clusters from dual-regression as well (*See*

Appendix, Results: Section A *for details*). Finally, we tested whether global WM microstructure of the right SLFT, as defined by the tractography measures, might also be driving the multimodal effects (*See* **Figure 6**). The results accordingly showed that average FA of the right SLFT, was positively associated total average intrinsic connectivity of the coSN (adj. $R^2 = 0.13$, $F(3, 29) = 2.62$, $p<0.01$) and pDMN (adj. $R^2 = 0.30$, $F(3, 29) = 5.47$, $p=0.001$**;** adj. $R^2 = 0.19$, $F(3, 29) = 3.48$, $p<0.01$), but negatively predicted the extrinsic connectivity between the fECN and the left Amygdala (adj. $R^2 = 0.09$, $F(3, 29) = 2.07$, $p<0.05$). In sum, both global and local microstructure of right SLFT primary and secondary fibers, along with a variety of other localized WM clusters, predicted within-network functional connectivity patterns of the triple-network associated with DR.

'Between-Network' Functional Connectivity and Depressive Rumination

FSLnets

Based on prior evidence for the role of the pDMN, coSN, and fECN in DR, we next used FSLnets to explore whether between-network functional connectivity of each pair combination of triple-network RSN's was associated with DR (*see* **METHODS: Between-Network Functional Connectivity**). That analysis revealed that DR severity was positively associated with an inverse correlation between the fECN and pDMN ($p<0.05$ FWE) (*See* **Figure 7**), and between the coSN and the pDMN ($p<0.01$ FWE). The third 'between-network' correlation between fECN and coSN was not significantly associated with DR in the discovery sample.

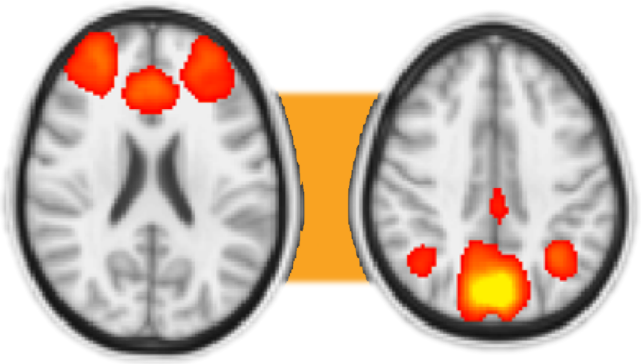

Figure 7: The above image depicts the fECN (*left*) and pDMN (*right*) whose inverse correlation was associated with DR severity ($p <0.05$ FWE).

452 ***WM Microstructure and 'Between-Network' Functional Connectivity***

453 As in the case of the within-
454 network functional connectivity
455 findings, we also sought to test
456 whether the global and local WM
457 biomarkers of DR predicted the
458 between-network inverse correlations
459 from FSLnets. Accordingly,
460 multimodal analysis revealed that
461 average global FA of the right SLFT,
462 predicted the coSN-pDMN inverse
463 correlation (adj. $R^2 = 0.15$, $F(3, 29) = 2.93$, $p<0.01$). Voxel-wise TBSS similarly revealed that the
464 DR-associated coSN-pDMN inverse correlation predicted lower FA of a medial cluster of the right
465 SLFT (adj. $R^2 = 0.17$, $F(3, 32) = 4.17$, $p<0.01$) and another along the right posterior Corona
466 Radiata ($p<0.01$ FWE)(*see red/yellow cluster* **Figure 8**). Correspondingly, FA of the left anterior
467 Corona Radiata negatively predicted the pDMN-fECN inverse correlation associated with DR.
468 ($p<0.05$, FWE) (*see blue and red clusters* **Figure 8**). Finally, we again used the ROI's created from
469 the significant TBSS clusters ($p=0.05$ FWE) to perform a similar non-voxelwise analysis so as to
470 explore whether atlas-defined divisions of WM clusters (i.e. discovered from our original TBSS
471 analysis with DR) might further clarify the nature of their association with between-network
472 functional connectivity. This approach showed that the DR-associated TBSS clusters of the CST,
473 CCG, ATR, UF, and Splenium each predicted the coSN-pDMN inverse correlation, whereas only
474 the left UF predicted the pDMN-fECN inverse correlation (*see* **Appendix, Results: Section B**).

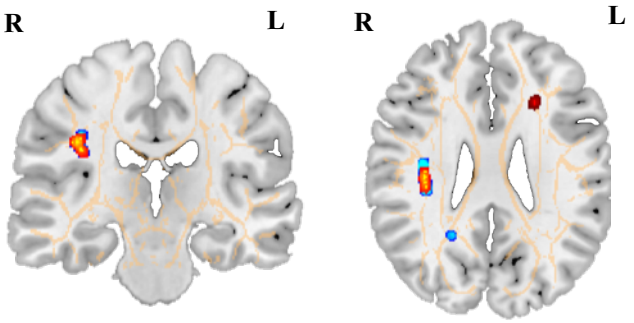

Figure 8: Lower FA of the right medial SLFT and the right posterior Corona Radiata (blue), as well as higher FA of right medial SLFT crossing fibers (red/yellow), was associated with greater pDMN-coSN inverse correlation. Similarly, greater FA of the left anterior Corona Radiata (red) was associated with greater pDMN-fECN inverse correlation.

In summary, the initial discovery sample revealed: 1) associations between DR severity and microstructure of the right-lateralized SLFT, along with localized WM clusters scattered throughout the SLFP, CCG, CST, ATR, Splenium, UF; 2) associations between DR severity and the microstructure of secondary fibers in the right superior Corona Radiata; 3) associations between DR severity and both intrinsic/extrinsic within-network functional connectivity of the triple-network; 4) associations between DR severity and between-network functional connectivity of the pDMN with each of the coSN and fECN of the triple-network; 5) associations between localized right medial SLFP primary and secondary-fiber microstructure and each manifestation of triple-network functional connectivity observed to sub-serve DR; 6) an association between right posterior Corona Radiata microstructure and the pDMN - coSN between-network functional connectivity found in (4) to sub-serve DR; 7) associations between left anterior Corona Radiata microstructure and the pDMN – fECN between-network functional connectivity found to sub-serve DR. 8) a variety of less prominent associations between localized WM clusters of the CST, CCG, ATR, UF, and Splenium, along with multiple manifestations of triple-network functional dysconnectivity found in (3) to sub-serve DR. *See* **Figure 9** for a visual summary.

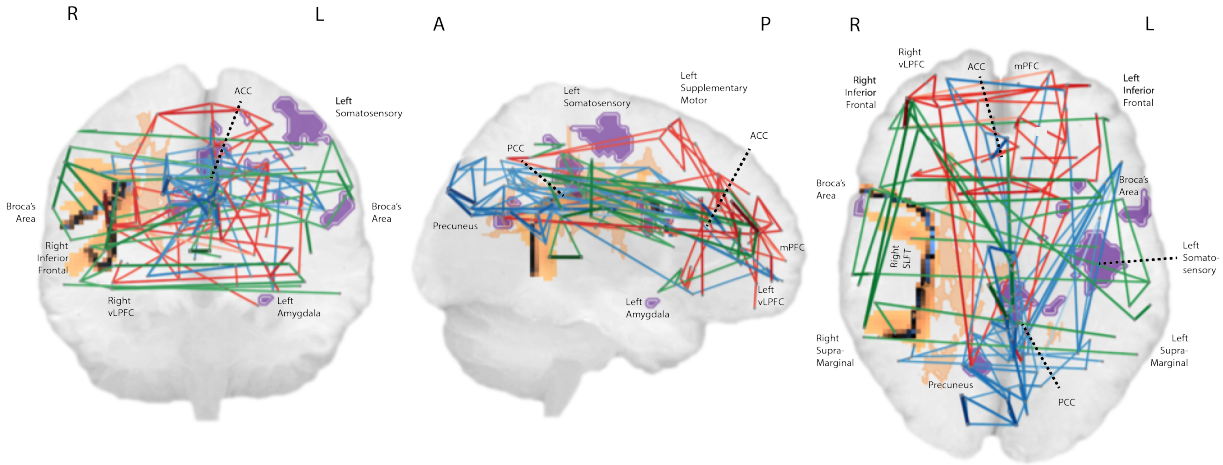

Figure 9: The above multimodal visualization summarizes key microstructural and functional connectivity biomarkers associated with DR in the discovery sample. WM tracts revealed both by TBSS and tractography are represented in copper heatmap. Regions whose within-network functional connectivity patterns are disrupted in DR are overlaid in purple. Finally, each of the pDMN, coSN, and fECN as a whole are here depicted as distinct networks with blue, green, and red edge connections, respectively.

RESULTS: REPLICATION SAMPLE

The replication sample exhibited similar descriptive statistics to those found in the discovery sample, but with some key differences. Perhaps most notably, for instance, depression severity was considerably milder on average in the replication sample (*M*=10.00, *SD*=6.18, range: 4-31, IQR=5.00). Furthermore, DR severity in the replication sample showed a significant positive skew, which we corrected using a log transformation to yield a normal distribution (Shapiro-Wilk = 0.948, $p = 0.07$). On the other hand, average DR severity overall was similar (*M*=11.00, *SD*=2.74, range: 7-20, IQR=2). Also, age exhibited a slight positive skew in the replication sample (*M*=31.36, *SD* = 5.79, Range: 22- 44), as in the discovery sample, along with a similar gender distribution (65% female). *See* **Table 1** for a summary comparing characteristics across initial and replication samples.

Sample Characteristics	Discovery Sample	Replication Sample
Age	*M* =27.51, *SD* = 8.80, Range: 18-55	*M* =31.36, *SD* = 5.79, Range: 22-44
Gender	22 females (56%)	24 females (65%)
DR Severity	*M* = 9.08, *SD* = 3.01	*M* =11.00, *SD* =2.74
Depressive Episodes	Moderate-severe MDD diagnosis only	Mild-severe MDD diagnosis, recurrent depression, dysphoria
Depression Severity	*M* = 31.94, *SD* = 8.16	*M* =10.00, *SD* =6.18
Medication Useage	Permitted if no medication change in the 12 weeks prior to study entry	Permitted if medications were reported as routine. 12-week stability data unavailable.
Other Psychopathology	No severe comorbidity	No severe comorbidity
Scanner Type	Siemens Skyra 3T	Siemens Tim Trio 3T
Multi-site?	No	Yes, 4 separate sites
dMRI parameters	TR/TE=1200/71.1, B=1000, 128 x 128 matrix, 3 mm slice thickness, anistropic voxels, 2 B0 + 53 DWI (55-directions)	TR/TE=2400/85, B=1500, 212 x 212 matrix, 2 mm slice thickness, isotropic voxels, 9 B0 + 128 DWI (137-directions)
rsfMRI parameters	eyes open, TR = 2000 ms, TE = 30 ms, 31 axial slices, voxel size = 3.125 x 3.125 x 3 mm^3 anisotropic	eyes open, TR = 2000 ms, TE = 30 ms, 40 axial slices, voxel size = 3 x 3 x 3 mm^3 isotropic

Table 1: The table above compares key characteristics across samples. In particular, the representation of age, gender, and DR severity was roughly equivalent across samples. On the other hand, the discovery sample included subjects with higher depression severity on average than those included in the replication sample. Although scanner manufacturer and strength was equivalent, the brands differed. Nevertheless, resampling procedures yielded dMRI and rsfMRI data with roughly equivalent core parameters including voxel dimensions, TR, and TE across samples.

Following the application of a nearly identical analytic methdology to that used with our original sample (*See* **METHODS: Replication**), we were able to fully replicate 49% of our cumulative findings across all methodologies, modalities, and levels of analysis. Specifically, twenty findings fully replicated, and two findings perhaps 'partially' replicated, out of forty retested models from the discovery sample.

Regression Findings (Predictor and Outcome)	Initial Sample	Replication Sample
Right SLFT Microstructure and DR Severity	TBSS (p<0.01 FWE, neg) Tractography (R^2=0.25, adj. R^2=0.18, neg)	TBSS (p<0.01 FWE, neg) Tractography (cond. R^2=0.37, neg)
Right SLFP Microstructure and DR Severity	TBSS (p<0.01 FWE, neg) Tractography (R^2=0.17, adj. R^2=0.05, neg)	TBSS (p<0.01 FWE, neg) Tractography (cond. R^2=0.23, neg)
CST Microstructure and DR Severity	TBSS (p<0.01 FWE, neg) Tractography (R^2=0.11, adj. R^2=0.06, neg)	TBSS (p<0.01 FWE, neg) Tractography (cond. R^2=0.17, neg)
CCG Microstructure and DR Severity	TBSS (p<0.05 FWE, neg)	TBSS (p<0.01 FWE, neg)
UF Microstructure and DR Severity	TBSS (p<0.05 FWE, neg)	TBSS (p<0.01 FWE, neg)
Splenium Microstructure and DR Severity	TBSS (p<0.05 FWE, neg)	TBSS (p<0.05 FWE, neg)
ATR Microstructure and DR Severity	TBSS (p<0.05 FWE, neg)	TBSS (p<0.05 FWE, neg)
pDMN Within-Network Connectivity and DR Severity	Dual-regression (p<0.01, FWE, neg)	Dual-regression (p<0.001 unc. ROI-analysis, neg)
fECN Within-Network Connectivity and DR Severity	Dual-regression (p<0.01, FWE, neg)	Dual-regression (p<0.001 unc. ROI-analysis, neg)
pDMN-fECN Between-Network Connectivity and DR Severity	FSLnets (p<0.05, FWE, neg)	FSLnets (p<0.01, FWE, neg)
Right SLFT Microstructure and pDMN Within-Network Connectivity	Tractography (R^2=0.36, adj. R^2=0.30, neg) TBSS (p<0.05 FWE, neg)	TBSS ROI-analysis (cond. R^2=0.36, neg)
Right SLFP Microstructure and pDMN Within-Network Connectivity	Tractography (R^2=0.26, adj. R^2=0.19, neg) TBSS (p<0.05 FWE, neg)	TBSS ROI-analysis (cond. R^2=0.33, neg)
ATR Microstructure and pDMN Within-Network Connectivity	TBSS ROI-analysis (R^2=0.33, adj. R^2=0.26, neg)	Tractography (cond. R^2=0.18, neg) TBSS ROI-analysis (cond. R^2=0.28, neg)
CCG Microstructure and pDMN Within-Network Connectivity	TBSS ROI-analysis (R^2=0.29, adj. R^2=0.22, neg)	Tractography (cond. R^2=0.12, neg) TBSS ROI-analysis (cond. R^2=0.21, neg)
Splenium Microstructure and pDMN Within-Network Connectivity	TBSS ROI-analysis (R^2=0.21, adj. R^2=0.12, neg)	TBSS ROI-analysis (cond. R^2=0.23, neg)
Right SLFT Microstructure and coSN Within-Network Connectivity	Tractography (R^2=0.21, adj. R^2=0.13, neg) TBSS (p<0.05 FWE, neg)	Tractography (adj. R^2=0.50, neg) TBSS (p<0.05 FWE, neg)
CCG Microstructure and coSN Within-Network Connectivity	TBSS ROI-analysis (R^2=0.27, adj. R^2=0.20, neg)	TBSS ROI-analysis (adj. R^2=0.26, neg)
Splenium Microstructure and coSN Within-Network Connectivity	TBSS ROI-analysis (R^2=0.17, adj. R^2=0.08, neg)	Tractography (cond. R^2=0.29, neg) TBSS ROI-analysis (cond. R^2=0.55, neg)
Right SLFT Microstructure and fECN Within-Network Connectivity	Tractography (R^2=0.18, adj. R^2=0.09, neg) TBSS (p<0.05 FWE, pos)	Tractography (cond. R^2=0.31, pos) TBSS ROI-analysis (cond. R^2=0.34, neg)
DR-associated WM microstructure and pDMN-fECN Between-Network Connectivity	FSLnets (p<0.05 FWE, pos)	FSLnets (p<0.05 FWE, pos)

Table 2: The above table depicts key findings (*left column*) that directly replicated across the discovery sample (*middle column*) and replication sample (right column). Each of the middle and right columns states the R^2 value from the respective regression models (adjusted in the discovery sample and conditional on both fixed and random effects in the replication sample), the methodology used to estimate that value (e.g. TBSS ROI-analysis, tractography, dual-regression, FSLnets), and the directionality of the relationship (*neg=negative,pos=positive*). In total, 20 unique findings out of 40 original findings directly replicated across samples.

523 ***dMRI Replications (TBSS and Tractography)***

524 The replication yielded a nearly equivalent set of dMRI findings using both TBSS and
525 tractography methods, with a striking degree of similarity in the voxelwise association between
526 WM microstructure and DR severity across samples. Using TBSS, we again found that FA of the

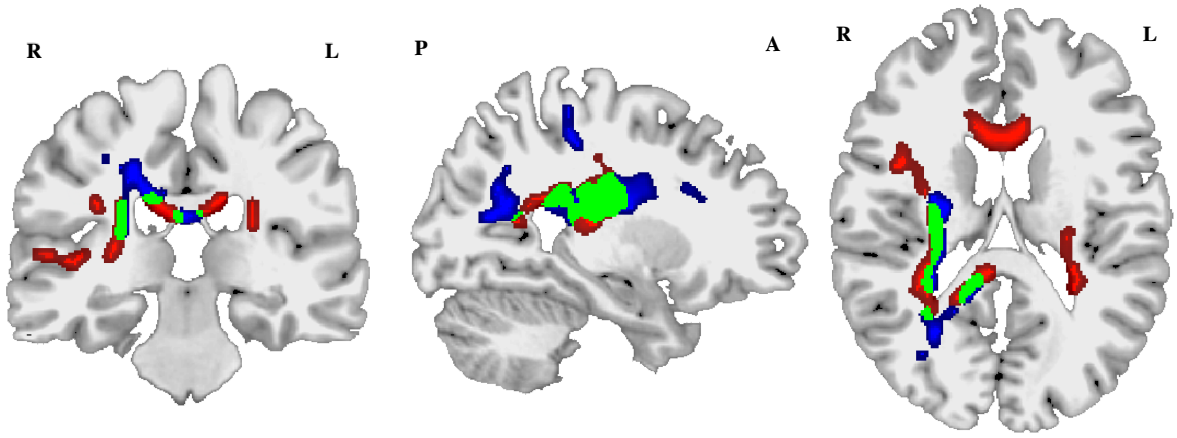

Figure 10: The above mosaic depict TBSS findings from the original sample (blue) and the NKI Rockland replication sample (red). The top row depicts the negative correlations in both samples between DR and FA (p=0.01 FWE in the discovery sample, p=0.05 FWE in the replication sample). These findings overlapped closely (green) along the right SLF and along the splenium. In the replication sample, there was slightly greater coverage, however, of the genu of the Corpus Callosum.

right SLFT, SLFP, CCG, CST, Splenium, UF, and ATR exhibited negative correlations with brooding scores (p<0.05, FWE)(*See* **Figure 10**). At the p=0.05 FWE threshold, 98 voxels, located in the right SLF, CST, and Corpus Callosum (*See top row* **Figure 10**), overlapped in this TBSS analysis across samples. The subsequent 'crossing-fibers' TBSS analysis, however, differed considerably across samples (*see* **Table 2 & Figure 10**). As in the discovery sample, however, the tractography replication demonstrated corresponding negative correlations between DR severity and average FA of localized WM clusters derived from the TBSS ROI-analysis. Additionally, the correlation between DR and global microstructure of the right SLFT was again the only tractography analysis that survived Bonferroni Correction for the six tracts tested (cond. $R^2 = 0.37$, $F(3, 35) = 8.90$, $p_{corrected}<0.05/6 = 0.0083$). As in the discovery sample, the effect of hemisphere was again significant with respect to the SLFT ($F(36,1)=5.43$, $p=0.03$), reiterating the right lateralization of this particular global WM biomarker. Whereas in the discovery sample, DR was also positively associated with microstructure of secondary-fibers in a small cluster of the right superior Corona Radiata, in the replication sample, it was negatively associated with microstructure of secondary-fibers of the Corpus Callosum and bilateral CST ($p < 0.05$ FWE). Although future replications would be needed to confirm, these differences may be largely attributable to the interaction between DR and depression severity across samples (*See* **Appendix, Results: Sections D & E**).

rsfMRI Replications (Dual-Regression and FSLnets)

Despite very similar microstructural connectivity findings across samples at whole-brain FWE-corrected thresholds (*See green overlapping clusters in* **Figure 10**), the initial within-network functional connectivity findings replicated only when using a small-volume ROI correction (i.e. MNI atlas-defined masks of significant regions from the discovery sample). Nevertheless, the results showed similar within-network functional connectivity patterns of the pDMN and fECN with respect to both anatomical location of intrinsic/extrinsic clusters and directionality (p<0.001) (*See correspondence of blue and red clusters in* **Figure 11**). Within the pDMN, lower intrinsic functional connectivity with the right precuneus replicated (p<0.001). The significant voxels of the pDMN and coSN whose functional connectivity was associated with DR were in close anatomical proximity across samples but not overlapping (*See correspondence of green clusters in* **Figure 11**), whereas 9 voxels of the fECN positive connectivity cluster in the left amygdala/ parahippocampal gyrus cluster were overlapping. The coSN also neuroanatomically tracked the within-network coSN effect observed discovery sample, but in the reverse direction (*See* **Appendix, Results: Section C** *for a discussion of 'partial' replications*).

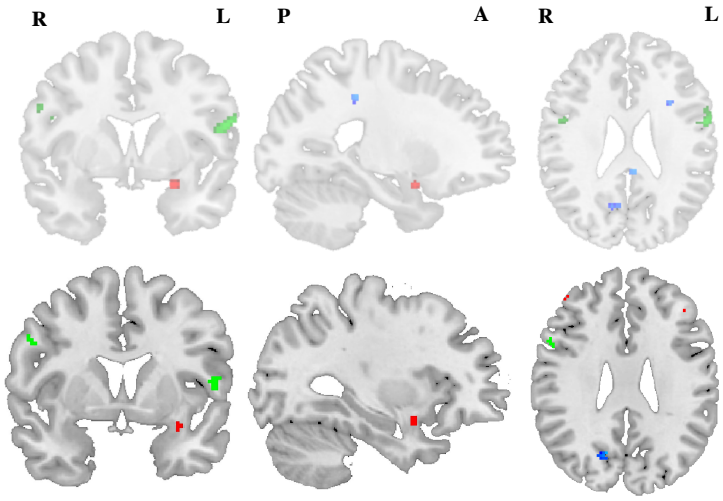

Figure 11: Within-network connectivity findings from the Rockland NKI replication sample (bottom row) compared to those from the initial samplediscovery sample (top row). Significant clusters exhibiting lower functional connectivity within the pDMN associated with DR are depicted in blue. Significant right anterior Insula clusters exhibiting lower functional connectivity within the coSN are depicted in light green, and the right superior Temporal Gyrus cluster exhibiting higher functional connectivity within the coSN is depicted in dark green (right bottom row). Finally, Ssignificant clusters exhibiting greater functional connectivity within the fECN are depicted in red and include the left Amygdala/ parahippocampal Gyrus. Finally, bilateral right anterior Insula clusters located in Broca's area that showed trending lower functional connectivity within the coSN are depicted in light green, and the right superior Temporal Gyrus cluster exhibiting higher functional connectivity within the coSN is depicted in dark green (right bottom row).

As with the microstructural findings, on the other hand, the between-network functional connectivity findings from FSLnets also replicated with FWE correction. Specifically, the association between DR and the pDMN-fECN inverse correlation fully replicated (p<0.05, FWE)(*See* **Figure 12**), whereas the coSN between-network associations with DR diverged across

samples (*See* **Appendix, Results: Section C**) in light of the reversed directionality of the coSN's within-network association with DR.

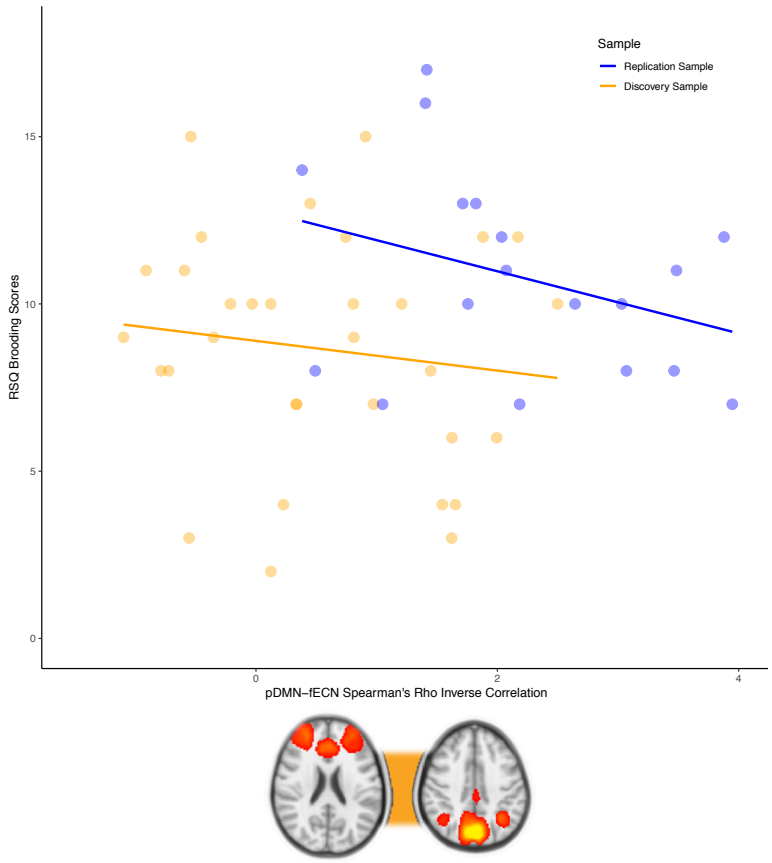

Figure 12: The scatterplot above depicts the association between pDMN-fECN inverse correlation and DR severity that was the one between-network functional connectivity relationship to fully replicate across samples.

Multimodal dMRI-rsfMRI Replications

Finally, when exploring multimodal microstructural-functional relationships in the replication sample, we found that global average FA of the right SLFT, along with localized WM clusters of the SLFP, CCG, ATR, and Splenium again predicted both the within-network and between-network functional connectivity biomarkers of DR (*see* **Table 2**). Importantly, the cumulative average FA measure from TBSS predicted pDMN-coSN between-network connectivity in the replication sample ($R^2 = 0.19$, $p<0.05$), despite there being no replication of the coSN-pDMN inverse correlation in association with DR. Also, global microstructure of the right SLFT and localized microstructure of the SLFP, CCG, ATR, and Splenium were again positively associated with the within-network functional connectivity of the pDMN and with corresponding directionality (cond. $R^2 = 0.36$, $p<0.05$; cond. $R^2 = 0.28$, $p<0.05$; cond. $R^2 = 0.33$, $p<0.05$; cond. $R^2 = 0.22$,

591 $p<0.05$). Additionally, the only fECN-related multimodal effect to replicate was the association
592 between localized right medial SLFT microstructure and fECN within-network connectivity. In
593 contrast, the relationship between WM microstructure and pDMN-fECN functional connectivity
594 across samples was ultimately non-specific to any single tract and implicated the cumulative DR-
595 associated TBSS clusters, as discovered through a final analysis in FSLnets ($p<0.05$).
596 We also found that global microstructure of the right SLFT and localized microstructure of
597 the CCG and Splenium were again positively associated with the within-network functional
598 connectivity of the coSN (cond. $R^2 = 0.50$, $p<0.05$; cond. $R^2 = 0.26$, $p<0.05$; cond. $R^2 = 0.55$,
599 $p<0.05$). Despite reversed directionality in DR's association with coSN within-network functional
600 connectivity, moreover, the directionality of multimodal relationships between WM microstructure
601 and coSN functional connectivity was nevertheless consistent across samples. Notably, secondary-
602 fiber microstructure also appeared to explain the between-network functional connectivity
603 differences across samples. Given that depression severity accordingly differed slightly across
604 samples (*See* **Table 1**), we conducted exploratory analysis to determine whether BDI scores might
605 explain the observed differences in secondary fiber microstructure and coSN functional connectivity
606 across samples (*See* **Appendix, Results: Sections D & E**).
607 In sum, our results ultimately showed that WM microstructure predicted 24-26% of the
608 variance in DR in both the discovery and replication samples, with the majority of the contribution
609 from global microstructure of the right SLFT. Between-network functional connectivity of the
610 triple-network alone also collectively predicted twice as much variance in DR (50-52%) in both the
611 discovery and replication samples, however, when controlling for WM microstructure. Furthermore,
612 our multimodal results indicated that microstructural connectivity of the SLFP, CCG, ATR, and
613 Splenium in particular largely accounted for the triple-network functional connectivity disturbances
614 associated with DR. Lastly, post-hoc analysis of replication-level False Discovery revealed a 0.1%
615 chance of all cross-modal replications being false-positives, and $\pi=0.795$ posterior-probability of
616 the replicated large effects being true positives (*See* **Appendix, Results: Section F**).
617
618
619
620
621
622

DISCUSSION

Overview

The neurobiology of trait Depressive Rumination (DR) is a heterogeneous network phenomenon. Replicated across two independent samples, findings from the present study conceptually converged across multiple dimensions of analysis. On the one hand, we found that compromised resting-state functional connectivity of the brain's 'triple-network' corresponding to self-referential, emotional salience, and attentional engagement processing, forms a functional neural basis for DR. On the other hand, we found that defective global and local frontoparietal White-Matter (WM) pathways confer microstructural risk factors for DR. Aligned without our initial hypotheses, we then observed strong evidence that these microstructural risk factors perpetuate the trait functional triple-network disorganization that defines DR.

Apart from differences in depression severity, discovery and replication samples were importantly matched on key behavioral characteristics: both comprised thirty-nine adults with equivalent measures of DR, similar demographic and inclusion criteria, and corresponding MRI data parameters following resampling procedures (*See* **Appendix, Methods: Sections F & G**). By directly replicating in this way, we created a unique analytic scenario whereby traditional hypothesis testing could be employed to test the generalizability of broader theories beyond individual findings. Principally among the fully-replicated functional connectivity findings, DR severity was negatively associated with within-network intrinsic connectivity of the Precuneal DMN (pDMN) and extrinsic connectivity of the frontal ECN (fECN) with the left Amygdala. DR severity was also negatively associated with a between-network inverse correlation of the pDMN and fECN. On the other hand, DR severity was associated with functional connectivity within the cingulo-opercular SN (coSN) as well as between the coSN and each of the pDMN and fECN; the precise configuration of those relationships differed across samples, however (*See* **Appendix, Results: Sections C & D**).

Microstructurally, DR severity was negatively associated with FA of a temporal section of the right SLFT, a robust finding that replicated across samples. Among the localized WM findings that replicated, we discovered that DR was strongly associated with localized WM clusters of the parietal SLF (SLFP), superior Corona Radiata (SCR), CCG, Corticospinal Tract (CST), Splenium, UF, and Anterior Thalamic Radiation (ATR). DR severity was also positively and negative associated with the microstructure of secondary "crossing" fibers in clusters that were largely localized to key junctures where the aforementioned primary-fiber pathways intersect.

Multimodally, microstructural biomarkers of DR that included global FA of the right SLFT, along with the localized CCG, ATR, and Splenium clusters, predicted the functional connectivity biomarkers of DR, both within and between the pDMN, coSN, and fECN. In contrast, the sample-specific secondary-fiber biomarkers of DR appeared to account for some of the observed variability in coSN functional connectivity across samples, but future studies will need to confirm this. To our knowledge, this is the first study to show that WM biomarkers of a behavioral measure predict within-network or between-network functional connectivity biomarkers of the same measure.

WM Microstructure and Depressive Rumination

A growing body of literature on the SLF – the WM biomarker found to most robustly track DR severity– suggests that its microstructure is associated with longer and more severe depressive episodes[102]. Deeper insights might be gleaned, however, from the more fine-grained analysis of the SLF conducted using multiple methodologies in the present study. Using both tractography and TBSS, we learned that DR was associated primarily, but not exclusively, with a specific subdivision of the SLF—an inferior portion connecting the middle/superior Temporal Gyrus with ipsilateral prefrontal/cingulo-opercular areas referred to as the SLFT, which most closely corresponds to SLF III – also known as the Arcuate Fasciculus. Neuroanatomically, the SLFT supplies fiber connections between Wernicke's area for speech production and Broca's area for language comprehension. The SLFT is most likely responsible for language communication between the parietal and frontal lobes, and specifically for maintaining phonological awarenes[103,104]. Accordingly, research on the microstructural basis of conduction aphasia has shown that SLFT deficits may be related to poor awareness of speech repetition[105]. In fact, mammals without vocal repetition ability do not have an SLFT[106]. As confirmed through tests of "hemisphericity" in both samples, moreover, microstructural deficits of the SLFT associated with DR were also distinctly right-lateralized. Although further research is needed, studies have begun to indicate that the right SLFT in particular may provide compensatory support for increased demands on language and higher cognitive thought[107,108]. Hence, the DR-associated language deficits of the right SLFT might reflect a lateralization of the WM pathways supporting internal versus external speech. Indeed, cortical areas connected by the right SLFT, such as the right Temporoparietal Junction and right superior Temporal Gyrus, have been implicated in internal speech faculties[9,109,110]. Hence, the SLFT deficits observed in the present study may allude to repetition defects of internal speech, and more broadly, the perseveration of self-referential language of thought[111], as a key maintaining factor for DR[112–114].

686 TBSS also revealed a strong association between DR and the microstructure of a variety of
687 localized WM clusters throughout the cortex, which highlights the distributed nature of DR as a
688 microstructural connectivity phenomenon. Additionally, the primary-fiber WM biomarkers were
689 largely consistent across samples, which suggests that these microstructural deficits in particular are
690 robust risk-factors for DR. In contrast, the secondary-fiber biomarkers revealed by TBSS were
691 largely variable across samples—a discrepancy that may be related to the interaction between
692 depression severity and DR (*See* **Appendix, Results: Sections D & E**), but will require future
693 studies with larger sample sizes to understand fully.
694 As our study indicates, these disturbances in WM microstructure manifest both locally (i.e.,
695 restricted to distinct clusters of WM) and globally (i.e., across the entirety of neuroanatomically
696 distinct fiber bundles such as the SLF) in DR. Still, it remains unclear whether both primary and
697 secondary WM biomarkers of DR reflect a trait-like vulnerability or develop over the course of
698 extended periods of persistent rumination. In support of the latter possibility, the "perseverative
699 cognition hypothesis"[54] posits that perseverative cognitive processes like rumination lead to a
700 prolonged stress response, which may further impact myelination patterns in both developing and
701 mature brains[115,116]. To the extent that the perseverative cognition of DR involves repetitive
702 cognitive processing, irregular myelination trajectories might accumulate over time in order to
703 sustain the excess cognitive load inflicted by DR.
704 ***Within-Network Functional Connectivity and Depressive Rumination***
705 The results from our functional connectivity analyses broadly implied that disrupted
706 integration and segregation of self-referential and cognitive control systems are associated with DR.
707 These patterns were firstly observed in the form of disrupted intrinsic and extrinsic functional
708 connectivity within each of the triple-network RSN's.
709 *pDMN*
710 The association between DR and functional connectivity within the pDMN was
711 characterized by two core features: 1) lower intrinsic connectivity with the right Precuneus; and 2)
712 lower extrinsic connectivity with the left Somatosensory Cortex, left inferior Frontal Gyrus, and left
713 Precentral Gyrus. Broadly speaking, diminished Precuneal integration with the DMN may reflect
714 impaired inhibition of internal mentation, particularly given the role of the Precuneus as a core
715 parietal hub for maintaining conscious self-awareness[117]. Conversely, greater segregation from
716 frontal cognitive control modules and somatosensory areas in DR may indicate globally
717 dysregulated self-referential processing that may also be detached from sensory experience[20,118,119].

718 *fECN*

719 Higher DR severity was also associated with greater extrinsic functional connectivity
720 between the fECN and the left Amygdala – a finding that replicated closely across samples and
721 might be explained in a number of ways. One interpretation stems from the premise that DR might
722 be construed as maladaptive coping strategy for avoiding the negative affective states experienced
723 in depression. For example, severe ruminators might repetitively reflect on their own cognitions as a
724 short-term attempt to ward off negative affect, but at the cost of maintaining a dysphoric mood in
725 the long term[13,92]. If DR were to accordingly operate *as though* it were adaptive, we might therefore
726 expect that it be accompanied by higher fECN-amygdala functional connectivity as a self-regulatory
727 measure[120]. This explanation also aligns with our multimodal findings that indicated that the
728 microstructure of the right SLFT may, to a certain extent, reinforce this pattern in a perseverative
729 manner. Nevertheless, functional connectivity of the fECN, in particular, proved to be the least
730 susceptible triple-network RSN to the impact of WM microstructure.

731 *coSN*

732 DR was also associated with functional connectivity of the coSN, and particularly with
733 clusters corresponding to Broca's area bilaterally. Although anatomically consistent across samples,
734 the direction of the relationship with DR and the specific sub-regions of Broca's area implicated
735 differed across samples. As one explanation for this discrepancy, emerging research offers a
736 compelling case that Broca's area has two distinct functional subunits: the first supports selective
737 language comprehension and the second is responsible for domain-general cognition[121]. Whereas the
738 selective language sub-region activates upon the presentation of salient semantic information, the
739 domain-general sub-region activates during more demanding multi-tasking scenarios. Not only can
740 these sub-regions operate more or less independently in response to multiple demands, their precise
741 anatomical boundaries appear to vary considerably across individuals[121,122]. Consequently, the
742 variable functional connectivity between the coSN and each of these versatile sub-regions might
743 indicate two potential "routes" to DR—excessive negative salience tagging of inner speech and/or
744 deficient positive salience toward reflective problem-solving. Accordingly, the multimodal findings
745 of the present study indicated that global microstructural deficits of the right SLFT predicted both of
746 these cases. Supportively, our exploratory tractography also revealed that the SLFT fibers actually
747 terminated in the vicinity of these coSN clusters in the majority of subjects.

748

749

750 ***Between-Network Functional Connectivity and Depressive Rumination***

751 Upon discovering spatially-overlapping patterns of aberrant extrinsic functional connectivity
752 among the triple-network RSNs, we further found that DR was associated with patterns of between-
753 network functional connectivity. Specifically, higher DR severity was associated with greater
754 inverse correlation between the pDMN-fECN in both discovery and replication samples, greater
755 inverse correlation between the coSN-pDMN in the discovery sample, and greater direct correlation
756 between the coSN-fECN in the replication sample.

757 *pDMN-fECN*

758 Not only did the pDMN-fECN findings replicate those of prior work[29,50], they also replicated
759 across both our initial and replication samples. Ultimately, this finding in particular underscores a
760 highly consistent pattern of antagonism between self-referential and cognitive control systems as a
761 defining feature of DR[103]. Since the pDMN is functionally coupled with the hippocampus during
762 memory retrieval[123], a greater pDMN-fECN inverse correlation associated with higher DR severity
763 could reflect a failure to regulate the episodic memory refreshing that is believed to occur during
764 self-referential processing[124]. More broadly, however, greater DMN-ECN coupling likely occurs
765 during task-related autobiographical planning[125]—a pattern that would appear to be antithetical to
766 DR. Ergo, greater pDMN-fECN inverse correlation associated with DR might conversely implicate
767 the decoupling of cortical midline hubs such as the PCC and ACC, whose synchrony is likely vital
768 to steering self-referential thought in the service of goal-directed cognition[46,104]. When the
769 integration and segregation patterns of these hubs become desynchronized, negatively-biased
770 internal mentation may in turn become increasingly difficult to regulate[50].

771 As with the multimodal relationships discovered when exploring each triple-network RSN
772 separately, tractography also revealed that right SLF microstructure alone predicted the pDMN-
773 fECN inverse correlation in both samples. This finding was surprising, given that the CCG also
774 supplies direct WM connections between ACC and PCC hubs of both networks. Nevertheless, a
775 recent study found that a disrupted SLF microstructure precluded efficient information transfer
776 between frontoparietal networks in hypertension patients[126]. In fact, the right SLF
777 neuroanatomically supplies lateral frontoparietal WM connections that could very well impact
778 pDMN-fECN synchronization patterns beyond the influence of more 'direct' cortical midline WM
779 pathways[52,127,128].

780

781

782 *coSN-pDMN and coSN-fECN*

783 Given that the SN is important for switching attention between externally and internally
784 salient stimuli[46,127], it is also known to interact with the DMN and ECN across contexts[52,127,128].
785 Accordingly, our findings indicated that abnormal between-network relationships with the pDMN
786 and fECN may confer variable risks for DR. As in the case of our within-network connectivity
787 findings, however, between-network connectivity patterns of the coSN also varied across samples,
788 which prevents us from forming hard interpretations about its precise role in DR (*See* **Appendix,**
789 **Results: Sections C, D, & E** *for exploratory analyses*). Interestingly, Hamilton et al. (2011)
790 observed a similar pattern of direction reversal with respect to the association DR severity and
791 between-network activation patterns of the SN as a function of depression severity[50]. Specifically,
792 their state-change analysis showed that relative to healthy controls, depressed participants displayed
793 increased SN activation at the onset of increases in ECN activity (and decreases in DMN activity);
794 in contrast, healthy controls exhibited increased SN response at the onset of increases in DMN
795 activity (and decreases in ECN activity). Thus, there is strong *a priori* evidence supporting the
796 notion that we should expect variable directionality in the relationship between DR severity and the
797 SN's connectivity profile among the triple-network RSN's. Along these lines, coSN-fECN and
798 coSN-pDMN between-network functional connectivity patterns proved to be clearly involved in
799 DR, since they were also associated with localized deficits of the right medial SLFT – a multimodal
800 finding that *was* consistent across samples.

801 ***Limitations and Generalizability***

802 One limitation of the present study may be that the neural biomarkers that it uncovered are
803 not purely attributable DR. Given how closely the theoretical constructs of DR and depression
804 severity are intertwined[80,129], however, there are fundamental theoretical and statistical obstacles to
805 establishing specificity of DR biomarkers in this context. Nevertheless, the majority of participants
806 included in our replication sample were dysphoric and/or depression-remitted, thereby enabling us
807 to at least infer that the replicated DR biomarkers are reproducibly observable across multiple
808 depressive disorder subtypes and at varying levels of depression severity.

809 By validating our initial findings with a replication sample, our study more importantly has
810 the unique advantage of contributing verifiably generalizable DR biomarkers to the larger corpus of
811 depression literature. Specifically, our study proposes a unified view of DR's neural
812 pathophysiology that is both sensitive to multiple network functional connectivity mechanisms and
813 conditional on microstructural connectivity risk factors[85,130,131]. Although twenty findings replicated

fully or partially, almost half of our findings did not. On the one hand, that level of discrepancy across samples echoes recent concerns in the neuroimaging community on issues related to reproducibility[132,133]. Indeed, those findings that did fully-replicate consisted only of large effects that were sufficiently powered to generalize as such. Along these lines, larger sample sizes would still be needed to validate the smaller-sized effects reported in supplement but not formally discussed. Nevertheless, our study clearly demonstrates that through the use of methodological triangulation along with an independent test-set, sub-optimal sample sizes can still be used resourcefully and powerfully to verify the generalizability of large effects.

CONCLUSION

In the present study, we aimed to identify functional and microstructural connectivity biomarkers of Depressive Rumination (DR), which we achieved in the form of twenty fully replicated findings across two independent samples. Our results from both data sets demonstrated that DR severity is associated with disorganized patterns of within-network and between-network functional connectivity of the 'triple-network', comprising the pDMN, coSN, and fECN. Further, DR severity is associated with microstructural dysconnectivity in the form of global WM deficits of the right temporal SLFT, along with deficits in localized clusters of primary and secondary WM fiber types distributed throughout the cortex. Perhaps most strikingly, however, these WM biomarkers predicted the abnormal functional connectivity patterns observed throughout the triple-network. Collectively, our findings powerfully corroborate our initial hypotheses and imply that emotionally dysregulated self-referential processing, perpetuated by inefficient attentional and language pathways, confers a set of multidimensional risk factors for trait DR.

Supported by initial discovery and replication, our study significantly unifies and extends research on the neurobiological substrates of trait rumination in depression. Ultimately, we demonstrate that neural pathophysiological models of trait DR are fundamentally multivariate, and should not, therefore, be reduced to singular or unimodal mechanisms as the field progresses. Rather, a precise and reproducible neurobiology of DR implores 'rethinking' it as a multimodal *system* of microstructural and functional triple-network brain mechanisms, whose whole is greater than the sum of its parts.

ACKNOWLEDGMENTS

The authors would first like to thank the technical staff at the Texas Advanced Computing Center (TACC) for supplying the computational resources and consulting that would have otherwise

rendered our neuroimaging analyses computationally intractable. We would also like to thank Ryan Hammonds for assistance with quality control of neuroimaging data. Additionally, the first author would also like to thank Ari Cohen for her incredible patience and support throughout drafting of the manuscript.

FUNDING

This work was supported by the R21 MH092430 award to Christopher G. Beevers.

COMPETING INTERESTS

We wish to confirm that there are no known conflicts of interest associated with this manuscript and there has been no significant financial support for this work that could have influenced its outcome.

MATERIALS AND CORRESPONDENCE

All materials and correspondence should be addressed to the first author, Derek Pisner, at dpisner@utexas.edu

REFERENCES

1. Beevers, C. G. Cognitive vulnerability to depression: A dual process model. *Clinical Psychology Review* **25,** 975–1002 (2005).
2. Nolen-Hoeksema, S. & Morrow, J. A prospective study of depression and posttraumatic stress symptoms after a natural disaster: the 1989 Loma Prieta Earthquake. *J. Pers. Soc. Psychol.* **61,** 115–121 (1991).
3. Nolen-hoeksema, S. Further Evidence for the Role of Psychosocial additional foci for future research . *Clin. Psychol. Sci. Pract.* **7,** 224–227 (2000).
4. Nolen-Hoeksema, S., Wisco, B. E. & Lyubomirsky, S. Rethinking Rumination. *Perspect. Psychol. Sci.* **3,** 400–424 (2008).
5. Watkins, E. Psychological treatment of depressive rumination. *Current Opinion in Psychology* **4,** 32–36 (2015).
6. Wells, A. & Papageorgiou, C. in *Depressive Rumination: Nature, Theory and Treatment* 259–273 (2008).
7. Woody, M. L. & Gibb, B. E. Integrating NIMH Research Domain Criteria (RDoC) into depression research. *Current Opinion in Psychology* **4,** 6–12 (2015).
8. Schnyer, D. M. *et al.* Neurocognitive therapeutics: from concept to application in the treatment of negative attention bias. *Biol. mood{&}anxiety Disord.* **5,** 1 (2015).
9. Nejad, A. B., Fossati, P. & Lemogne, C. Self-referential processing, rumination, and cortical midline structures in major depression. *Front. Hum. Neurosci.* **7,** 666 (2013).
10. Yoshimura, S. *et al.* Self-referential processing of negative stimuli within the ventral anterior cingulate gyrus and right amygdala. *Brain Cogn.* **69,** 218–225 (2009).
11. Brewer, J. A., Garrison, K. A. & Whitfield-Gabrieli, S. What about the "Self" is Processed in the Posterior Cingulate Cortex? *Front. Hum. Neurosci.* **7,** (2013).
12. Kühn, S., Vanderhasselt, M. A., De Raedt, R. & Gallinat, J. Why ruminators won't stop: The structural and resting state correlates of rumination and its relation to depression. *J. Affect. Disord.* **141,** 352–360 (2012).
13. Watkins, E. & Teasdale, J. D. Rumination and overgeneral memory in depression: Effects of self-focus and analytic thinking. *J. Abnorm. Psychol.* **110,** 353–357 (2001).
14. Buckner, R. L. & Carroll, D. C. Self-projection and the brain. *Trends Cogn. Sci.* (2007).
15. Laurita, A. C., Hazan, C. & Spreng, R. N. Dissociable patterns of brain activity for mentalizing about known others: A role for attachment. *Soc. Cogn. Affect. Neurosci.* (2017).
16. Freton, M. *et al.* The eye of the self: Precuneus volume and visual perspective during autobiographical memory retrieval. *Brain Struct. Funct.* (2014).
17. Ahmed, S. *et al.* Association between precuneus volume and autobiographical memory impairment in posterior cortical atrophy: Beyond the visual syndrome. *NeuroImage Clin.* (2018).
18. Ye (叶群), Q., Zou (邹富渟), F., Lau (劉克頑), H., Hu (胡谊), Y. & Kwok (郭思齊), S. C. Causal evidence for mnemonic metacognition in human precuneus. *J. Neurosci.* (2018).
19. McCurdy, L. Y. *et al.* Anatomical Coupling between Distinct Metacognitive Systems for Memory and Visual Perception. *J. Neurosci.* (2013).
20. Rosenbaum, D. *et al.* Aberrant functional connectivity in depression as an index of state and trait rumination. *Sci. Rep.* **7,** 2174 (2017).
21. Northoff, G. *et al.* Self-referential processing in our brain-A meta-analysis of imaging studies on the self. *Neuroimage* **31,** 440–457 (2006).
22. Greicius, M. D., Krasnow, B., Reiss, A. L. & Menon, V. Functional connectivity in the resting brain: a network analysis of the default mode hypothesis. *Proc. Natl. Acad. Sci. U. S. A.* **100,** 253–258 (2003).
23. Utevsky, A. V., Smith, D. V. & Huettel, S. A. Precuneus Is a Functional Core of the Default-Mode Network. *J. Neurosci.* **34,** 932–940 (2014).
24. Whitfield-Gabrieli, S. *et al.* Associations and dissociations between default and self-reference networks in the human brain. *Neuroimage* (2011).
25. Sheline, Y. I. *et al.* The default mode network and self-referential processes in depression. *Proc. Natl. Acad. Sci. U. S. A.* **106,** 1942–1947 (2009).
26. Leech, R., Kamourieh, S., Beckmann, C. F. & Sharp, D. J. Fractionating the default mode network: distinct contributions of the ventral and dorsal posterior cingulate cortex to cognitive control. *J. Neurosci.* **31,** 3217–24 (2011).
27. Wang, X., Öngür, D., Auerbach, R. P. & Yao, S. Cognitive Vulnerability to Major Depression: View from the Intrinsic Network and Cross-network Interactions. *Harv. Rev. Psychiatry* **24,** 188–201 (2016).

28. Jilka, S. R. *et al*. Damage to the Salience Network and Interactions with the Default Mode Network. *J. Neurosci*. **34,** 10798–10807 (2014).
29. Liang, X. *et al*. Interactions between the Salience and Default-Mode Networks Are Disrupted in Cocaine Addiction. *J. Neurosci*. **35,** 8081–8090 (2015).
30. Siegle, G. J., Steinhauer, S. R., Thase, M. E., Stenger, V. A. & Carter, C. S. Can't shake that feeling: Event-related fMRI assessment of sustained amygdala activity in response to emotional information in depressed individuals. *Biol. Psychiatry* **51,** 693–707 (2002).
31. LeDoux, J. The emotional brain, fear, and the amygdala. *Cellular and Molecular Neurobiology* **23,** 727–738 (2003).
32. Etkin, a, Egner, T. & Kalisch, R. Emotional processing in anterior cingulate and medial prefrontal. *Trends Cogn. Sci*. **15,** 85–93 (2011).
33. Cooney, R. E., Joormann, J., Eugène, F., Dennis, E. L. & Gotlib, I. H. Neural correlates of rumination in depression. *Cogn. Affect. Behav. Neurosci*. **10,** 470–8 (2010).
34. Kolling, N., Behrens, T. E. J., Wittmann, M. K. & Rushworth, M. F. S. Multiple signals in anterior cingulate cortex. *Curr. Opin. Neurobiol*. **37,** 36–43 (2016).
35. Stevens, F. L., Hurley, R. A. & Taber, K. H. Anterior Cingulate Cortex: Unique Role in Cognition and Emotion. *J. Neuropsychiatry Clin. Neurosci*. **23,** 121–125 (2011).
36. Ordaz, S. J. *et al*. Ruminative brooding is associated with salience network coherence in early pubertal youth. *Soc. Cogn. Affect. Neurosci*. nsw133 (2016).
37. Bernstein, E. E., Heeren, A. & McNally, R. J. Unpacking Rumination and Executive Control: A Network Perspective. *Clin. Psychol. Sci*. (2017).
38. Yang, Y. *et al*. Task and resting-state fMRI reveal altered salience responses to positive stimuli in patients with major depressive disorder. *PLoS One* **11,** 1–19 (2016).
39. Kocsel, N. *et al*. Trait Rumination Influences Neural Correlates of the Anticipation but Not the Consumption Phase of Reward Processing. *Front. Behav. Neurosci*. **11,** (2017).
40. Southworth, F., Grafton, B., MacLeod, C. & Watkins, E. Heightened ruminative disposition is associated with impaired attentional disengagement from negative relative to positive information: support for the "impaired disengagement" hypothesis. *Cogn. Emot*. **31,** 422–434 (2017).
41. Koster, E. H. W., De Lissnyder, E., Derakshan, N. & De Raedt, R. Understanding depressive rumination from a cognitive science perspective: The impaired disengagement hypothesis. *Clinical Psychology Review* **31,** 138–145 (2011).
42. Grafton, B., Southworth, F., Watkins, E. R. & MacLeod, C. Stuck in a sad place: Biased attentional disengagement in rumination. *Emotion* **16,** 63–72 (2016).
43. Rude, S. S., Maestas, K. L. & Neff, K. Paying attention to distress: What's wrong with rumination? *Cogn. Emot*. **21,** 843–864 (2007).
44. Wang, K. *et al*. Individual differences in rumination in healthy and depressive samples: Association with brain structure, functional connectivity and depression. *Psychol. Med*. **45,** 2999–3008 (2015).
45. Jacobs, R. H. *et al*. Targeting ruminative thinking in adolescents at risk for depressive relapse: Rumination-focused cognitive behavior therapy in a pilot randomized controlled trial with resting state fMRI. *PLoS One* **11,** (2016).
46. Menon, V. Large-scale brain networks and psychopathology: A unifying triple network model. *Trends in Cognitive Sciences* **15,** 483–506 (2011).
47. Wu, X. *et al*. A triple network connectivity study of large-scale brain systems in cognitively normal APOE4 carriers. *Front. Aging Neurosci*. **8,** (2016).
48. Liu, Y. *et al*. Decreased Triple Network Connectivity in Patients with Recent Onset Post-Traumatic Stress Disorder after a Single Prolonged Trauma Exposure. *Sci. Rep*. **7,** (2017).
49. Zheng, H. *et al*. The altered triple networks interaction in depression under resting state based on graph theory. *Biomed Res. Int*. **2015,** (2015).
50. Hamilton, J. P. *et al*. Default-mode and task-positive network activity in major depressive disorder: Implications for adaptive and maladaptive rumination. *Biol. Psychiatry* **70,** 327–333 (2011).
51. Burkhouse, K. L. *et al*. Neural correlates of rumination in adolescents with remitted major depressive disorder and healthy controls. *Cogn. Affect. Behav. Neurosci*. **17,** 394–405 (2017).
52. Menon, V. & Uddin, L. Q. Saliency, switching, attention and control: a network model of insula function. *Brain Struct. Funct*. **214,** 655–667 (2010).
53. Zuo, N. *et al*. White matter abnormalities in major depression: A tract-based spatial statistics and rumination study. *PLoS One* **7,** (2012).

54. Brosschot, J. F., Gerin, W. & Thayer, J. F. The perseverative cognition hypothesis: A review of worry, prolonged stress-related physiological activation, and health. *Journal of Psychosomatic Research* (2006).
55. Peer, M., Nitzan, M., Bick, A. S., Levin, N. & Arzy, S. Evidence for Functional Networks within the Human Brain's White Matter. *J. Neurosci.* (2017).
56. Mezer, A., Yovel, Y., Pasternak, O., Gorfine, T. & Assaf, Y. Cluster analysis of resting-state fMRI time series. *Neuroimage* (2009).
57. Yendiki, A. *et al.* Automated probabilistic reconstruction of white-matter pathways in health and disease using an atlas of the underlying anatomy. *Front. Neuroinform.* **5,** 23 (2011).
58. Tao, Y. *et al.* The Structural Connectivity Pattern of the Default Mode Network and Its Association with Memory and Anxiety. *Front. Neuroanat.* **9,** (2015).
59. Steffens, D. C., Taylor, W. D., Denny, K. L., Bergman, S. R. & Wang, L. Structural integrity of the uncinate fasciculus and resting state functional connectivity of the ventral prefrontal cortex in late life depression. *PLoS One* **6,** (2011).
60. Pennebaker, J. W. & King, L. a. Linguistic styles: Language use as an individual difference. *J. Pers. Soc. Psychol.* **77,** 1296–1312 (1999).
61. Crinion, J. T. *et al.* Neuroanatomical markers of speaking Chinese. *Hum. Brain Mapp.* **30,** 4108–4115 (2009).
62. Monnart, A., Kornreich, C., Verbanck, P. & Campanella, S. Just swap out of negative vibes? Rumination and inhibition deficits in major depressive disorder: Data from event-related potentials studies. *Frontiers in Psychology* **7,** (2016).
63. Hamilton, J. P., Farmer, M., Fogelman, P. & Gotlib, I. H. Depressive Rumination, the Default-Mode Network, and the Dark Matter of Clinical Neuroscience. *Biological Psychiatry* **78,** 224–230 (2015).
64. Chavez, R. S. & Heatherton, T. F. Multimodal frontostriatal connectivity underlies individual differences in self-esteem. *Soc. Cogn. Affect. Neurosci.* (2013).
65. Medaglia, J. D. *et al.* Functional Alignment with Anatomical Networks is Associated with Cognitive Flexibility. 1–38 (2016).
66. Braun, U. *et al.* From Maps to Multi-dimensional Network Mechanisms of Mental Disorders. *Neuron* **97,** 14–31 (2018).
67. Bassett, D. S. & Gazzaniga, M. S. Understanding complexity in the human brain. *Trends in Cognitive Sciences* **15,** 200–209 (2011).
68. Mandell, D., Siegle, G. J., Shutt, L., Feldmiller, J. & Thase, M. E. Neural substrates of trait ruminations in depression. *J. Abnorm. Psychol.* **123,** 35–48 (2014).
69. Bagby, R. M., Rector, N. A., Bacchiochi, J. R. & McBride, C. The stability of the response styles questionnaire rumination scale in a sample of patients with major depression. *Cognitive Therapy and Research* **28,** 527–538 (2004).
70. Fawcett, J. M. *et al.* The origins of repetitive thought in rumination: Separating cognitive style from deficits in inhibitory control over memory. *J. Behav. Ther. Exp. Psychiatry* **47,** 1–8 (2015).
71. Button, K. S. *et al.* Power failure: Why small sample size undermines the reliability of neuroscience. *Nat. Rev. Neurosci.* **14,** 365–376 (2013).
72. Mulugeta, L. *et al.* Credibility, Replicability, and Reproducibility in Simulation for Biomedicine and Clinical Applications in Neuroscience Credibility in Simulation for Biomedicine and Clinical Applications. **12,** 1–16 (2018).
73. Poldrack, R. A. *et al.* Scanning the horizon: Towards transparent and reproducible neuroimaging research. *Nat. Rev. Neurosci.* **18,** 115–126 (2017).
74. Parlatini, V. *et al.* Functional segregation and integration within fronto-parietal networks. *Neuroimage* **146,** 367–375 (2017).
75. Nooner, K. B. *et al.* The NKI-Rockland sample: A model for accelerating the pace of discovery science in psychiatry. *Frontiers in Neuroscience* (2012).
76. Sheehan, D. V. *et al.* The Mini-International Neuropsychiatric Interview (M.I.N.I.): The development and validation of a structured diagnostic psychiatric interview for DSM-IV and ICD-10. in *Journal of Clinical Psychiatry* **59,** 22–33 (1998).
77. First, M. B., Gibbon, M., Spitzer, R. L., Gibbon, M. & Williams, J. B. W. in *American Psychiatric Press, Inc.* (1997).
78. Beevers, C. G., Clasen, P. C., Enock, P. M. & Schnyer, D. M. Attention bias modification for major depressive disorder: Effects on attention bias, resting state connectivity, and symptom change. *J. Abnorm. Psychol.* **124,** 463–475 (2015).

79. Erdur-Bakera, Ö. ¨ & Bugaya, A. The short version of ruminative response scale: Reliability, validity and its relation to psychological symptoms. in *Procedia - Social and Behavioral Sciences* **5,** 2178–2181 (2010).
80. Treynor, W., Gonzalez, R. & Nolen-Hoeksema, S. Rumination reconsidered: A psychometric analysis. *Cognit. Ther. Res.* **27,** 247–259 (2003).
81. Beck, A., Steer, R. & Brown, G. Beck Depression Inventory-II. *San Antonio* 12–15 (1996).
82. Jenkinson, M., Beckmann, C. F., Behrens, T. E. J., Woolrich, M. W. & Smith, S. M. FSL. *NeuroImage* **62,** 782–790 (2012).
83. Smith, S. M. *et al.* Tract-based spatial statistics: Voxelwise analysis of multi-subject diffusion data. *Neuroimage* **31,** 1487–1505 (2006).
84. Jbabdi, S., Behrens, T. E. J. & Smith, S. M. Crossing fibres in tract-based spatial statistics. *Neuroimage* **49,** 249–256 (2010).
85. Westlye, L. T. *et al.* Life-span changes of the human brain white matter: diffusion tensor imaging (DTI) and volumetry. *Cereb. Cortex* **20,** 2055–2068 (2010).
86. Nolen-Hoeksema, S. Sex Differences in Unipolar Depression: Evidence and Theory. *Psychological Bulletin* **101,** 259–282 (1987).
87. De Groot, M. *et al.* Improving alignment in Tract-based spatial statistics: Evaluation and optimization of image registration. *Neuroimage* **76,** 400–411 (2013).
88. Torgerson, C. M. *et al.* DTI tractography and white matter fiber tract characteristics in euthymic bipolar I patients and healthy control subjects. *Brain Imaging Behav.* **7,** 129–139 (2013).
89. Vernooij, M. W. *et al.* Fiber density asymmetry of the arcuate fasciculus in relation to functional hemispheric language lateralization in both right- and left-handed healthy subjects: A combined fMRI and DTI study. *Neuroimage* **35,** 1064–1076 (2007).
90. Beckmann, Mackay, Filippini & Smith. Group comparison of resting-state FMRI data using multi-subject ICA and dual regression. *Neuroimage* **47,** S148 (2009).
91. Thomas Yeo, B. T. *et al.* The organization of the human cerebral cortex estimated by intrinsic functional connectivity. *J. Neurophysiol.* **106,** 1125–1165 (2011).
92. Watkins, E. & Brown, R. G. Rumination and executive function in depression: an experimental study. *J. Neurol. Neurosurg. Psychiatry* **72,** 400–2 (2002).
93. Dutta, A., McKie, S. & Deakin, J. F. W. Resting state networks in major depressive disorder. *Psychiatry Res.* **224,** 139–51 (2014).
94. Smith, S. M. The future of FMRI connectivity. *NeuroImage* **62,** 1257–1266 (2012).
95. Smith, S. M. & Nichols, T. E. Threshold-free cluster enhancement: Addressing problems of smoothing, threshold dependence and localisation in cluster inference. *Neuroimage* **44,** 83–98 (2009).
96. Smith, S. FSLnets. *FMRIB Software Library v5.0* Available at: https://fsl.fmrib.ox.ac.uk/fsl/fslwiki/FSLNets.
97. First, M. B. et, Spitzer, R. L., Gibbon, M. & Williams, J. B. W. *Structured Clinical Interview for DSM-IV Axis I Disorders, Clinician Version (SCID-CV). for DSMIV* (1997).
98. Berle, D. & Moulds, M. L. Emotional Reasoning Processes and Dysphoric Mood: Cross-Sectional and Prospective Relationships. *PLoS One* (2013).
99. Williams, A. D. & Moulds, M. L. Investigation of the indulgence cycles hypothesis of suppression on experimentally induced visual intrusions in dysphoria. *Behav. Res. Ther.* (2007).
100. Gouttard, S., Styner, M., Prastawa, M., Piven, J. & Gerig, G. Assessment of reliability of multi-site neuroimaging via traveling phantom study. in *Lecture Notes in Computer Science (including subseries Lecture Notes in Artificial Intelligence and Lecture Notes in Bioinformatics)* (2008).
101. Bowring, A., Maumet, C. & Nichols, T. Exploring the Impact of Analysis Software on Task fMRI Results. *bioRxiv* (2018).
102. Lai, C. H. & Wu, Y. T. Alterations in white matter micro-integrity of the superior longitudinal fasciculus and anterior thalamic radiation of young adult patients with depression. *Psychol. Med.* **44,** 2825–2832 (2014).
103. Jenkins, L. M. *et al.* Shared white matter alterations across emotional disorders: A voxel-based meta-analysis of fractional anisotropy. *NeuroImage Clin.* **12,** 1022–1034 (2016).
104. Oechslin, M. S., Imfeld, A., Loenneker, T., Meyer, M. & Jäncke, L. The plasticity of the superior longitudinal fasciculus as a function of musical expertise: a diffusion tensor imaging study. *Front. Hum. Neurosci.* **3,** 76 (2009).
105. Bernal, B. & Ardila, A. The role of the arcuate fasciculus in conduction aphasia. *Brain* **132,** 2309–2316 (2009).

106. Schmahmann, J. D. *et al*. Association fibre pathways of the brain: Parallel observations from diffusion spectrum imaging and autoradiography. *Brain* (2007).
107. Glasser, M. F. & Rilling, J. K. DTI tractography of the human brain's language pathways. *Cereb. Cortex* **18,** 2471–2482 (2008).
108. Lindell, A. K. In your right mind: Right hemisphere contributions to language processing and production. *Neuropsychol. Rev.* **16,** 131–148 (2006).
109. Geva, S. *et al*. The neural correlates of inner speech defined by voxel-based lesion-symptom mapping. *Brain* **134,** 3071–3082 (2011).
110. Alderson-Day, B. & Fernyhough, C. Inner speech: Development, cognitive functions, phenomenology, and neurobiology. *Psychol. Bull.* **141,** 931–965 (2015).
111. Fodor, J. A. *The Language of Thought. Philosophical Books* (1975).
112. Bernblum, R. & Mor, N. Rumination and Emotion-Related Biases in Refreshing Information. *Emotion* **10,** 423–432 (2010).
113. Aldao, A., Mennin, D. S. & McLaughlin, K. A. Differentiating worry and rumination: Evidence from heart rate variability during spontaneous regulation. *Cognit. Ther. Res.* **37,** 613–619 (2013).
114. Nolen-Hoeksema, S. in *Ruminative thoughts*. 135–144 (1996).
115. Nugent, K. L. *et al*. Cortisol reactivity to stress and its association with white matter integrity in adults with schizophrenia. *Psychosom. Med.* (2015).
116. Sheikh, H. I. *et al*. Links between white matter microstructure and cortisol reactivity to stress in early childhood: Evidence for moderation by parenting. *NeuroImage Clin.* (2014).
117. Klaassens, B. L. *et al*. Diminished Posterior Precuneus Connectivity with the Default Mode Network Differentiates Normal Aging from Alzheimer's Disease. *Front. Aging Neurosci.* **9,** 97 (2017).
118. Johnson, M. K., Nolen-Hoeksema, S., Mitchell, K. J. & Levin, Y. Medial cortex activity, self-reflection and depression. *Soc. Cogn. Affect. Neurosci.* **4,** 313–327 (2009).
119. Pelletier-Baldelli, A., Bernard, J. A. & Mittal, V. A. Intrinsic functional connectivity in salience and default mode networks and aberrant social processes in youth at ultra-high risk for psychosis. *PLoS One* **10,** (2015).
120. Cohen, N. *et al*. Using executive control training to suppress amygdala reactivity to aversive information. *Neuroimage* **125,** 1022–1031 (2016).
121. Fedorenko, E., Duncan, J. & Kanwisher, N. Language-selective and domain-general regions lie side by side within Broca's area. *Curr. Biol.* (2012).
122. Fedorenko, E. & Varley, R. Language and thought are not the same thing: Evidence from neuroimaging and neurological patients. *Ann. N. Y. Acad. Sci.* (2016).
123. Huijbers, W., Pennartz, C. M. A., Cabeza, R. & Daselaar, S. M. The hippocampus is coupled with the default network during memory retrieval but not during memory encoding. *PLoS One* **6,** (2011).
124. Züst, M. A. *et al*. Hippocampus is place of interaction between unconscious and conscious memories. *PLoS One* **10,** (2015).
125. Spreng, R. N., Stevens, W. D., Chamberlain, J. P., Gilmore, A. W. & Schacter, D. L. Default network activity, coupled with the frontoparietal control network, supports goal-directed cognition. *Neuroimage* (2010).
126. Li, X. *et al*. Disrupted Frontoparietal Network Mediates White Matter Structure Dysfunction Associated with Cognitive Decline in Hypertension Patients. *J. Neurosci.* (2015).
127. Uddin, L. Q. Salience Network Dysfunction. *Salience Netw. Hum. Brain* 23–28 (2017).
128. Uddin, L. Q. Salience processing and insular cortical function and dysfunction. *Nat. Rev. Neurosci.* **16,** 55–61 (2014).
129. Roelofs, J., Muris, P., Huibers, M., Peeters, F. & Arntz, A. On the measurement of rumination: A psychometric evaluation of the ruminative response scale and the rumination on sadness scale in undergraduates. *J. Behav. Ther. Exp. Psychiatry* **37,** 299–313 (2006).
130. Inano, S., Takao, H., Hayashi, N., Abe, O. & Ohtomo, K. Effects of Age and Gender on White Matter Integrity. *Am. J. Neuroradiol.* **32,** 2103–2109 (2011).
131. Zorlu, N. *et al*. Abnormal white matter integrity and decision-making deficits in alcohol dependence. *Psychiatry Res. - Neuroimaging* **214,** 382–388 (2013).
132. Eklund, A., Nichols, T. E. & Knutsson, H. Cluster failure: Why fMRI inferences for spatial extent have inflated false-positive rates. *Proc. Natl. Acad. Sci.* (2016).
133. Evans, S. What Has Replication Ever Done for Us? Insights from Neuroimaging of Speech Perception. *Front. Hum. Neurosci.* (2017).